Hochschule für Angewandte Wissenschaften Hamburg
Hamburg University of Applied Sciences

Bachelor Thesis

Model-based evaluation of experimental modal analysis methods for multi-axis base excitation

Author: Dimitrij Shulkin
Course of studies: Maschinenbau / Entwicklung und Konstruktion
Date of submission: 21. August 2012
First examiner: Prof. Dr.-Ing. habil. Frank Ihlenburg
Second examiner: Dipl.-Ing. (FH) M.Sc. Christian Busch

Hochschule für Angewandte Wissenschaften Hamburg
Hamburg University of Applied Sciences

Hochschule für Angewandte Wissenschaften Hamburg
Fakultät Technik und Informatik
Department Maschinenbau und Produktion
Berliner Tor 9
20099 Hamburg

in Zusammenarbeit mit:

AIRBUS Operations GmbH
Loads & Aeroelastics - EGLCRZ
Kreetslag 10
21129 Hamburg

Verfasser: Dimitrij Shulkin
Matrikelnummer: 1929784
Abgabedatum: 21.08.2012

1. Prüfer: Prof. Dr.-Ing. habil. Frank Ihlenburg
2. Prüfer: Dipl.-Ing. M. Sc. Christian Busch

Industrielle Betreuer: Dipl.-Ing. M. Sc. Christian Busch

Hochschule für Angewandte Wissenschaften Hamburg
Hamburg University of Applied Sciences

Abstract

The multi-axis shaker is often used for the dynamic qualification of aerospace structures. The vibration test data can also be used for extracting of modal parameters like eigenfrequencies, mode shapes and damping. This thesis presents such identification method called ISSPA (Identification of Structural Systems Parameters) that disregards the unsolicited motions of the shaker during the vibration test. These unwanted motions are the consequence of the interaction (cross-talk) between the shaker and the test structure. To understand a dynamic behaviour of the test structure because of cross-talk effects a 3D demo structure is programmed with MATLAB and simulated in the frequency domain. The analytical acceleration responses and geometry properties of the demo structure are retained as input data to check the ability of the ISSPA that is implemented in MATLAB. Finally, the identification procedures are applied to the real vibration test data of an aircraft section in order to identify the modal parameters that can be used for the validation of analytical models.

Hochschule für Angewandte Wissenschaften Hamburg
Hamburg University of Applied Sciences

Eidesstattliche Erklärung

Hiermit versichere ich, dass ich die Bachelorthesis selbstständig verfasst und keine anderen als die angegebenen Quellen und Hilfsmittel benutzt habe, alle Ausführungen, die anderen Schriften wörtlich oder sinngemäß entnommen wurden, kenntlich gemacht sind und die Arbeit in gleicher oder ähnlicher Fassung noch nicht Bestandteil einer Studien- oder Prüfungsleistung war.

Unterschrift des Verfassers

Hochschule für Angewandte Wissenschaften Hamburg
Hamburg University of Applied Sciences

Aufgabenstellung

In der Arbeit sollen analytische Methoden zur experimentellen Modalanalyse untersucht und implementiert werden, wobei der Fokus auf der modalen Identifikation im Frequenzbereich liegt. Dabei sind insbesondere mehrachsigen Basisbeschleunigungen als Strukturanregung zu berücksichtigen, wie sie bei hydraulischen Schütteltischen auftreten. Messungen haben gezeigt, dass eine einachsige Anregung der Schütteltische oft zu einer mehrachsigen Basisbeschleunigung führt, was auf die dynamischen Eigenschaften des Tisches selbst zurückzuführen ist. Die korrekte Identifikation des Prüflings wird hierdurch erschwert. Insbesondere ist die ISSPA Methode zu betrachten, die von der Universität Kassel in Zusammenarbeit mit dem DLR entwickelt und erprobt wurde.

Das Ziel der Arbeit ist die modale Identifikation einer realen Flugzeug-Sektion auf Basis experimentell ermittelter Vibrationsdaten. Die Methodik soll zunächst an einem virtuellen Demonstrations-Modell erprobt werden, welches typischen Leichtbaustrukturen der Luftfahrt hinsichtlich Frequenznachbarschaften und Dämpfungskopplung ähnelt. Die daraus gewonnenen Erkenntnisse sind dann auf reale Messdaten eines Vibrations-Großversuches anzuwenden. Hierbei ist von besonderem Interesse, ob die Eigenschwingungsformen der Flugzeug-Sektion identifizierbar und frei von offensichtlichen dynamischen Eigenschaften des Schütteltisches sind.

Contents

List of Figures

List of Tables

List of Symbols

Matrices and vectors

$[A]$	Real part acceleration frequency response matrix
$[A_u]$	Real part acceleration excitation matrix
$[B]$	Imaginary part acceleration frequency response matrix
$[B_u]$	Imaginary part acceleration excitation matrix
$[\tilde{B}]$	Substitute measuring matrix
$[C]$	Damping matrix
$[C_g]$	Generalized damping matrix
$[C^*]$	Mass-modified damping matrix
$[\bar{C}_g]$	Equivalent generalized damping matrix
$[\hat{C}^*]$	Condensed mass -modified damping matrix
$[E]$	Expanding matrix
$[G]$	Time independent geometry matrix
$[\tilde{G}]$	Local geometry matrix
$[H(\omega)]$	Frequency response matrix
$[I]$	Unit matrix
$[\tilde{I}]$	Substitute pseudo-unit matrix
$[K]$	Stiffness matrix
$[K_g]$	Generalized stiffness matrix
$[\hat{K}^*]$	Condensed mass-modified stiffness matrix
$[\widetilde{K}]$	Element stiffness matrix
$[M]$	Mass matrix
$[M_g]$	Generalized mass matrix
$[\widetilde{M}]$	Local lumped mass matrix
$[\overline{M}_g]$	Diagonal matrix of orthogonality condition
$[S_B]$	Singular eigenvalues matrix
$[\tilde{S}_B]$	Reduced singular value matrix
$[T]$	3D-space transformation matrix
$[T_{sc}]$	Static condensation’s transformation matrix

$[\tilde{V}]$	Transformation matrix for the substitute measurement matrices
$[X]$	Left-hand modal matrix
$[Y]$	Mode shape matrix
$[\phi]$	Mass-normalized mode shape matrix
$[\Omega]$	Angular velocity matrix
$[\omega]$	Diagonal excitation frequency matrix
$[{\omega_0}^2]$	Diagonal eigenvalue matrix
$\{d\}$	Position vector of non-deformed structure in the relative system
$\{F_{eff}\}$	Effective force vector
$\{\tilde{F}_{eff}\}$	Local effective force vector
$\{X\}$	Left-hand eigenvector
$\{\tilde{X}\}$	Condensed left-hand eigenvector
$\{Y\}$	Right-hand eigenvector
$\{\tilde{Y}\}$	Condensed right-hand eigenvector
$\{f\}$	Force vector
$\{\ddot{q}\}$	Acceleration in the modal space
$\{r\}$	Position vector of deformed structural nodes in the relative system
$\{\dot{r}\}$	Relative velocity vector
$\{\ddot{r}\}$	Relative acceleration of the structural node *j*
$\{u\}$	Absolute position vector
$\{u_b\}$	Absolute displacement of the relative system
$\{\dot{u}\}$	Absolute velocity vector
$\{\dot{u}_b\}$	Base velocity
$\{\ddot{u}\}$	Absolute acceleration vector
$\{\ddot{u}_0\}$	Base acceleration
$\{v\}$	Relative position of deformed structural nodes
$\{\dot{v}\}$	Relative velocity of deformed structural nodes
$\{\ddot{v}\}$	Relative acceleration of deformed structural nodes
$\{\Omega\}$	Rotation of the basis

Scalars

E_{kin}	Kinetic energy
E_{pot}	Potential energy
J	Hamilton's definite integral
L	Lagrangian function
M	Torque
S	Single external force
W	Virtual work
W_{nc}	Virtual work of non conservative forces
$c_{\ g}$	Generalized damping
$\bar{c}_g$	Equivalent generalized damping
c_H	Condition number
f	Eigenfrequency
i	$\sqrt{-1}$
j	Structural node or degree of freedom
m	Number of excitation frequency points
m_g	Generalized mass
$\bar{m}_g$	Equivalent generalized mass
p	Number of structural nodes or degrees of freedom
r	Number of effective degrees of freedom or effective modes
φ	Rotational degree of freedom
s	Singular value
t	Time
κ	Relation factor
δ	Damping coefficient
ζ	Modal damping
λ	Damped eigenvalue
ω	Excitation angular frequency
ω_d	Damped angular eigenfrequency
ω_0	Angular eigenfrequency
${\omega_0}^2$	Undamped eigenvalue

Indices and special symbols

$A \dots J$	Sensors of the demo structure
Im	Imaginary part
Re	Real part
$3D$	Three-dimensional
b	Basis
ex	Exact
i	Local structural nodal point in chapter 4
id	Identified
j	j_{th} structural node or degree of freedom
n	n_{th} excitation frequency point
sc	Static condensation
$shaker$	Corresponding to the shaker
$struct$	Corresponding to the structure
$[\dots]^{+}$	Pseudo-inverse matrix
$[\dots]_{p,p}$	Matrix of the p,p-dimension
$[\hat{\dots}]$	Condensed matrix
$[\dots_{global}]$	Global matrix
$\{\dots\}$	Column vector
$\{\dots\}^{T}$	Row vector
$\{\dots_{global}\}$	Global vector
$\{\dots_{p}\}$	Primary coordinates vector
$\{\dots_{s}\}$	Secondary coordinates vector
$diag(\dots)$	Diagonal matrix

List of Abbreviations

DOF	Degree of freedom
FEM	Finite-element method
FRF	Frequency response function
ISSPA	Identification of Structural System Parameters
MAC	Modal Assurance Criterion
MDOF	Multi-degree-of-freedom
R&T	Research and technology

1 Introduction

The aircraft industry is constantly seeking for improving the quality of vibration tests. Most important objectives are the reduction in the testing times and the accuracy of the vibration test data. Vibration tests on a multi-axial shaking table are often used for the dynamic qualification to control if a structure is able to resist a vibration environment in its service life. In most cases the additional information on the structural modal parameters like eigenfrequencies, mode shapes, generalized mass, stiffness and damping can be extract from the same vibration test data. The identified modal parameters within the same test set-up enable the validation of analytical models.

The test structure has to be attached on a shaker table and excited with harmonic excitation in all spatial degrees of freedom (DOF). The measured data are the multi-axial base acceleration and the structural responses. The shaker table interacts with the structure during the test that results in an unsolicited motion of the shaker. The influence of this cross-talk has to be considered by modal identification methods. The identification method ISSPA (Identification of Structural System Parameters) represents an opportunity to the modal survey test where the cross-talk effects can be disregarded.

The object of this thesis is the implementation of such identification method (ISSPA) with MATLAB-environment and applying at first to the analytical demo-structure and finally to real vibration data of the original aircraft section. The test data are descended within the frame of an Airbus research and technology project.

In chapter 2 the Hamilton's principle for the single mass is introduced. The Hamilton approach is used for the derivation of the simplified equation of motion for base excited multi degree-of-freedom (MDOF) systems. The equation of motion forms the basis for the theoretical modal analysis.

Chapter 3 describes the experimental test environments in details. Beginning with some important dynamical components of the shaker the interaction between the test structures is presented. Subsequently the identification method (ISSPA) is in details explained. The theory is implemented with the MATLAB-function *identification.m* that allows the calculation of the eigenfrequencies, mode shapes and damping.

Chapter 4 covers the architecture of the three-dimensional (3D) base excited demo-structure. The finite-element (FEM) procedures like derivation of system matrices and reduction of redundant DOFs are performed with programmed MATLAB-function *demostructure.m.* The additional programmed function *response_analysis.m* accomplishes the simulation of the base excitation of the demo structure. Especially the crass-talk effects are investigated. The demo-structure will be retained for the check of the ability of ISSPA.

Chapter 5 firstly presents the application of *identification.m* to the analytical acceleration response data of the demo-structure. The sensitivity and accuracy of *ISSPA* with respect to conditions that represent many practical test situations is checked. Finally *identification.m* is applied to the vibration test data of the original aircraft section in order to identify the modal parameter.

2 Basic Formulations for Base Excited Structures

This chapter is focused at first on derivation of equation of motion for base-excited structures. Beginning with the single mass the classical mechanical principles like Newtonian law, d'Alembert's principle and Hamilton's principle are introduced.

The formulations for the single mass may to be extended for multi-degree-of-freedom (MDOF) systems. The Hamilton's principle is applied to the base-excited MDOF systems to derive the equation of motion.

At last the equations of motion give the basis to introduce the fundamentals of theoretical modal analysis. Modal analysis is a process of determining the inherent dynamic characteristics of a system in forms of eigenfrequencies, damping factors and mode shapes, and using them to formulate a mathematical model for its dynamic behaviour [10]. The theoretical equation of acceleration responses of MDOF systems is shown because these magnitudes are measured in the following vibration test.

2.1 Single Mass

The intrinsic physical properties of any linear elastic structural system subjected to an external source of excitation are its mass, elastic properties, and energy-loss mechanism or damping. Each of these properties is assumed to be concentrated in a single physical element [10].

2.1.1 Newtonian law

The equation of motion of the single mass represents expressions of Newton's second law of motion, which defines that the rate of change of momentum of mass particle *m* is equal to a force acting on it. This relationship can be expressed mathematically by the differential equation [2]

$$\{f\} = \frac{d}{dt}\left(m\frac{d\{u\}}{dt}\right) \tag{2.1}$$

where f is the time dependent applied force vector and $\{u\}$ is the time dependent position vector of single mass *m*. For most problems in structural dynamics it may be assumed that mass does not vary with time, in which case eq. **(2.1)** may be written as

$$\{f\} = m\frac{d^2\{u\}}{dt^2} = m\{\ddot{u}\} \tag{2.2}$$

where the dots represent differentiation corresponding to time.

2.1.2 D 'Alembert's principle

The eq. **(2.2**) can be reformulated as follows

$$\{f\} - m\{\ddot{u}\} = 0 \tag{2.3}$$

where the second term is called the inertial force resisting the acceleration of the mass. The eq. **(2.3)** is the expression of the d 'Alembert's principle that says that the addition of the inertial force to the other acting forces evokes equilibrium [2].

The requirement for the equilibrium is that the total virtual work of all forces vanishes. This requirement contains virtual displacements, and is thus equally appropriable to mass at rest and to mass in motion. D 'Alembert's principle can be now rephrased as follows: the total virtual work of the impressed forces, amplified by the inertia forces, vanishes for reversible displacements [2]

$$\delta W = (\{f\} - m\{\ddot{u}\})\delta u = 0 \tag{2.4}$$

A given system of impressed forces will generally not be in equilibrium. This requires the satisfaction of special conditions. The total virtual work of the impressed forces will usually be different zero. In that case the motion of the system makes up for the deficiency. The mass moves in such a way that the additional inertial forces, caused by the motion, bring the balance up to zero. In this case d'Alembert's principle gives the equation of motion of an arbitrary single mass [12].

2.1.3 Hamilton's principle

By multiplying eq. **(2.4)** by dt and an integration with respect to the time

$$\int_{t_1}^{t_2} \delta W dt = \int_{t_1}^{t_2} (\{f\} - m\{\ddot{u}\})\delta u dt = 0 \tag{2.5}$$

the total virtual work done by the impressed forces and forces of inertia can be transformed into a true variation [12]. D'Alemebert's principle can thus be mathematically reformulated as Hamilton's principle. This requires that a definite integral

$$J = \int_{t_1}^{t_2} (L + W_{nc}) dt \tag{2.6}$$

of the Lagrangian function

$$L = E_{kin} - E_{pot} \tag{2.7}$$

where L is the difference between the kinetic and potential energies of the single mass in addition with the work of non conservative forces W_{nc}, shall be stationary for arbitrary possible variations of the configurations of the mass:

$$\delta J = \delta \int_{t_0}^{t_1} (E_{kin} - E_{pot} + W_{nc}) dt = 0 \tag{2.8}$$

where the initial and final configurations of the mass must be prescribed

2.2 Multi-Degree-of-Freedom Systems

In aforementioned sections Newton's law, virtual-work approach and Hamilton's principle were introduced. These methods can be used to derive the equation of motion of MDOF system. For many mechanical and structural systems, more than one coordinate is needed to describe its motion and vibration sufficiently. The result is a MDOF model. Such a model characterizes a system in terms of mass, stiffness and damping matrices [10].

The following section is focused on the derivation of the equation of motion under the base excitation using Hamilton's principle according to [7] and [11]. Subsequently a theoretical modal analysis for MDOF systems will be presented according to [4] and [10].

2.2.1 Base excitation

The system matrices $[M]$, $[K]$ and $[C]$ of the MDOF system as shown in Figure 2.1 can be found after the discretization of the continuum body using a finite element method [7]. The vector $\{f\}$ contains external loads that are moving with the base.

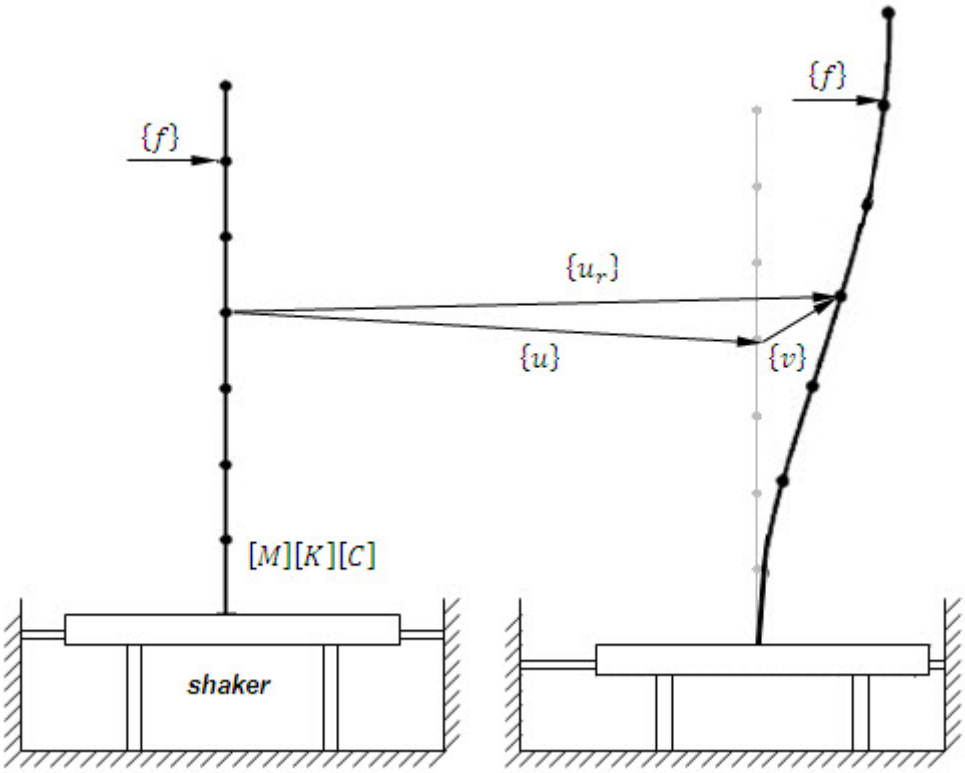

Figure 2.1. Base excitation

The kinetic energy E_{kin} under the base excitation depends on the absolute velocity $\{\dot{u}\}$

$$E_{kin} = \frac{1}{2}\{\dot{u}\}^T[M]\{\dot{u}\} \tag{2.9}$$

The potential energy E_{pot} only consists of deformation energy of the system that can be described using relative motion $\{v\}$

$$E_{pot} = \frac{1}{2}\{v\}^T[K]\{v\} \tag{2.10}$$

The work done by non-conservative forces is given by

$$W_{nc} = \{v\}^T\{f\} - \{v\}^T[C]\{\dot{v}\} \tag{2.11}$$

One notices that the kinetic energy of the system depends on the whole motion, while the potential energy and the work done by the non conservative forces depend on the relative motion alone. Since the absolute motion of non deformed system is always known, the variation of the energy terms involved in Hamilton's principle must be followed with respect to the relative motion. For the variation of the potential energy follows

$$\delta E_{pot} = \delta\{v\}^T \frac{\partial E_{pot}}{\partial\{v\}} = \delta\{v\}^T[K]\{v\} \tag{2.12}$$

Because the whole velocity variation is equal to the relative motion variation $\delta\{\dot{u}\}^T = \delta\{\dot{v}\}^T$ for the variation of the kinetic energy follows

$$\delta E_{kin} = \delta\{\dot{u}\}^T \frac{\partial E_{pot}}{\partial\{\dot{u}\}} = \delta\{\dot{v}\}^T[K]\{\dot{u}\} \tag{2.13}$$

The variation of the work done by non conservative forces gives

$$\delta W_{nc} = \delta\{v\}^T \frac{\partial W_{nc}}{\partial\{v\}} = \partial\{v\}^T(\{f\} - [C]\{\dot{v}\}) \tag{2.14}$$

Substituting the equations **(2.12)**, **(2.13)** and **(2.14)** into the eq. **(2.8)** gives

$$\int_{t_1}^{t_2} \delta\{v\}^T(-[M]\{\ddot{u}\} - [C]\{\dot{v}\} - [K]\{v\} + \{f\})dt = 0 \tag{2.15}$$

For the equations of motion of the MDOF system under base excitation and external loads follows

$$[M]\{\ddot{u}\} + [C]\{\dot{v}\} + [K]\{v\} = \{f\} \tag{2.16}$$

2.2.2 General equation of motion of base-excited MDOF systems

The overall displacement of the structure consists of the absolute displacement of non-deformed structure due to the support motion and elastic structural deformations. Since the dynamical behaviour of

the structure depends on the time motions of the structural deformations that are significant to the system moving with the structure, it is necessary to introduce a relative system as shown in Figure 2.2 that moves with the support.

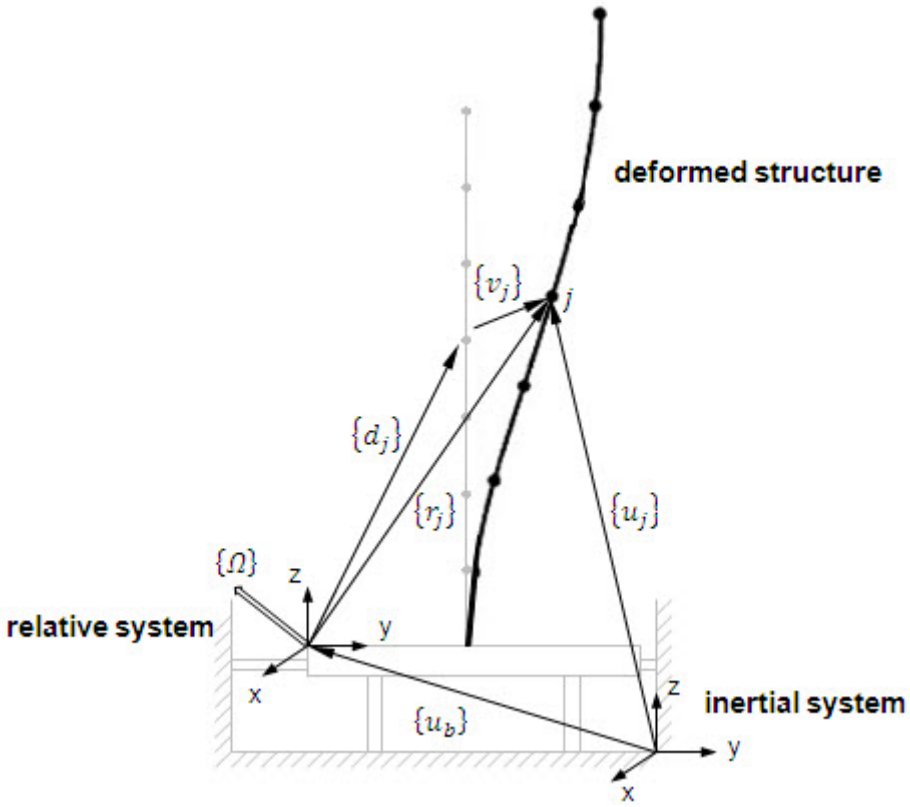

Figure 2.2: MDOF structure and relative system

The vector $\{u_b\}$ involves the absolute displacement of the relative system on the base, i.e. the origin of the relative coordinate system. The vector $\{\Omega\}$ describes the rotation of the basis. The position of an arbitrary discrete structural node j of the deformed structure is given by the vector $\{r_j\}$. The location of a general structural node j is given for the deformed structure by

$$\{u_j\} = \{u_b\} + \{r_j\} \tag{2.17}$$

The derivation of eq. **(2.17)** gives the velocity in matrix formulation

$$\{\dot{u}_j\} = \{\dot{u}_b\} + [\tilde{\Omega}]\{r_j\} + \{\dot{r}_j\} \tag{2.18}$$

where

$$[\tilde{\Omega}] = \begin{bmatrix} 0 & -\Omega_z & \Omega_y \\ \Omega_z & 0 & -\Omega_x \\ -\Omega_y & \Omega_x & 0 \end{bmatrix} \tag{2.19}$$

For all structural nodes $j = 1,2, \dots p$ follows

$$\begin{Bmatrix} \{\dot{u}_1\} \\ \vdots \\ \{\dot{u}_p\} \end{Bmatrix} = \begin{bmatrix} [I] \\ \vdots \\ [I] \end{bmatrix} \{\dot{u}_b\} + \begin{bmatrix} [\tilde{\Omega}] & [0] & [0] \\ [0] & \ddots & [0] \\ [0] & [0] & [\tilde{\Omega}] \end{bmatrix} \begin{Bmatrix} \{r_1\} \\ \vdots \\ \{r_p\} \end{Bmatrix} + \begin{Bmatrix} \{\dot{r}_1\} \\ \vdots \\ \{\dot{r}_p\} \end{Bmatrix} \tag{2.20}$$

or in generally form

$$\{\dot{u}\} = [E]\{\dot{u}_b\} + [\Omega]\{r\} + \{\dot{r}\} \tag{2.21}$$

The vectors $\{\dot{u}\}$, $\{r\}$ and $\{\dot{r}\}$ contain parts of all structural nodes, the matrix $[E]$ expands the base velocities $\{\dot{u}_b\}$ to all structural nodes and the matrix $[\Omega]$ expands the velocities due to the base rotation to all structural nodes.

The derivation of eq. **(2.21)** gives the acceleration

$$\{\ddot{u}\} = \{\ddot{r}\} + [E]\{\ddot{u}_b\} + [\dot{\Omega}]\{r\} + [\Omega][\Omega]\{r\} + 2[\Omega]\{\dot{r}\} \tag{2.22}$$

The vector $\{r_j\}$ can be composed of the vector of the structural node j in the relative coordinate system $\{d_j\}$ and by the deformation of the structure $\{v_j\}$:

$$\{r_j\} = \{d_j\} + \{v_j\} \tag{2.23}$$

Because of $\{d_j\} = const.$ for the derivations follows

$$\{\dot{r}_j\} = \{\dot{v}_j\} \; and \; \{\ddot{r}_j\} = \{\ddot{v}_j\} \tag{2.24}$$

Due to the very small structural deformations, the vector $\{v_j\}$ can be disregarded when compared with $\{d_j\}$

$$\{r_j\} = \{d_j\} + \{v_j\} \approx \{d_j\} \tag{2.25}$$

Expanding of equations **(2.23)**, **(2.24)** and **(2.25)** for all structural nodes $j = 1,2, \dots p$ and substituting them into eq. **(2.22)** gives the expression

$$\{\ddot{u}\} = \{\ddot{v}\} + [E]\{\ddot{u}_b\} + [\dot{\Omega}]\{d\} + [\Omega][\Omega]\{d\} + 2[\Omega]\{\dot{v}\} \tag{2.26}$$

This equation contains relations of the relative kinematics for all structural nodes. The absolute accelerations of arbitrary structural nodes consist of

- the relative acceleration $\{\ddot{v}\}$,
- the acceleration of the origin ordinates of the relative system $[E]\{\ddot{u}_b\}$,

- the tangential acceleration $[\dot{\Omega}]\{d\}$,
- the centripetal acceleration $[\Omega][\Omega]\{d\}$ and
- the Coriolis acceleration $2[\Omega]\{\dot{v}\}$.

Substituting of equations **(2.26)** into eq. **(2.16)** and sorting gives the general equation of motion for base-excited MDOF systems

$$[M]\{\ddot{v}\} + (2[\Omega][M] + [C])\{\dot{v}\} + [K]\{v\} = \{f\} - [M]\left([E]\{\ddot{u}_b\} + [\dot{\Omega}]\{d\} + [\Omega][\Omega]\{d\}\right) \tag{2.27}$$

2.2.3 Simplified equation of motion of base-excited MDOF systems

As shown in [7], in most practical cases where the rotational velocity remains small, the Coriolis acceleration as well as the centripetal acceleration can be disregarded. For the absolute acceleration of the structure follows

$$\{\ddot{u}\} = \{\ddot{v}\} + [E]\{\ddot{u}_b\} + [\dot{\Omega}]\{d\} \tag{2.28}$$

or of the arbitrary structural node *j*

$$\{\ddot{u}_j\} = \{\ddot{v}_j\} + \{\ddot{u}_b\} + [\tilde{\dot{\Omega}}]\{d_j\} \tag{2.29}$$

where

$$[\tilde{\dot{\Omega}}]\{d_j\} = \begin{bmatrix} 0 & -\dot{\Omega}_z & \dot{\Omega}_y \\ \dot{\Omega}_z & 0 & -\dot{\Omega}_x \\ -\dot{\Omega}_y & \dot{\Omega}_x & 0 \end{bmatrix} \begin{Bmatrix} d_{jx} \\ d_{jy} \\ d_{jz} \end{Bmatrix} \tag{2.30}$$

can be rewritten as follows

$$[\tilde{\dot{\Omega}}]\{d_j\} = \begin{bmatrix} 0 & d_{jz} & -d_{jy} \\ -d_{jz} & 0 & d_{jx} \\ d_{jy} & -d_{jx} & 0 \end{bmatrix} \begin{Bmatrix} \dot{\Omega}_x \\ \dot{\Omega}_y \\ \dot{\Omega}_z \end{Bmatrix} \tag{2.31}$$

or in generally form

$$[\tilde{\dot{\Omega}}]\{d_j\} = [D_j]\{\dot{\Omega}\} \tag{2.32}$$

With the vector of angular velocity $[\Omega]$ that constitutes the derivations of the base rotational motions $\{\varphi\}$

$$[\Omega] = \begin{Bmatrix} \Omega_x \\ \Omega_y \\ \Omega_z \end{Bmatrix} = \begin{Bmatrix} \dot{\varphi}_{bx} \\ \dot{\varphi}_{by} \\ \dot{\varphi}_{bz} \end{Bmatrix} = \{\dot{\varphi}_b\} \tag{2.33}$$

eq. **(2.29)** can be written as

$$\{\ddot{u}_j\} = \{\ddot{v}_j\} + \{\ddot{u}_b\} + [D_j]\{\ddot{\varphi}_b\} \tag{2.34}$$

Expanding eq. **(2.34)** for all structural nodes on the structure $j = 1,2, \dots p$ gives

$$\begin{Bmatrix} \{\ddot{u}_1\} \\ \vdots \\ \{\ddot{u}_p\} \end{Bmatrix} = \begin{Bmatrix} \{\ddot{v}_1\} \\ \vdots \\ \{\ddot{v}_p\} \end{Bmatrix} + \begin{bmatrix} [I] & [D_1] \\ \vdots & \vdots \\ [I] & [D_p] \end{bmatrix} \begin{Bmatrix} \{\ddot{u}_b\} \\ \{\ddot{\varphi}_b\} \end{Bmatrix} \tag{2.35}$$

or in generally form

$$\{\ddot{u}\} = \{\ddot{v}\} + [G]\{\ddot{u}_0\} \tag{2.36}$$

where

- $\{\ddot{u}\}$ is the absolute acceleration vector for all structural nodes,
- $\{\ddot{v}\}$ is the relative acceleration vector for all structural nodes,
- $[G]$ is the time independent geometry matrix that transforms the predefined rigid motions cause of base acceleration $\{\ddot{u}_0\}$ into acceleration $[E]\{\ddot{u}_b\}$ of the relative origin ordinates and tangential acceleration $[D]\{\ddot{\varphi}_b\}$ to all structural nodes. It means that the all structural nodes contain the components of the rigid body motion producing by the shaker! The columns of $[G]$ can be interpreted as rigid body displacements due to the translational and rotational base motions.
- $\{\ddot{u}_0\}$ is the base acceleration vector.

Substituting of equations **(2.36)** into eq. **(2.16)** gives the simplified equation of motion for base-excited MDOF systems

$$[M]\{\ddot{v}\} + [C]\{\dot{v}\} + [K]\{v\} = \{f\} - [M][G]\{\ddot{u}_0\} = \{F_{eff}\} \tag{2.37}$$

This equation shows that the structural vibrations are induced by inertia forces which caused by the multi-axis base excitation $\{\ddot{u}_0\}$ and external loads. The vibrations occur as motions relative to the co-ordinate system, which is moving with the relative vibration table.

2.2.4 Modal analysis of base-excited MDOF systems

Considering the undamped free vibration solution of the eq. **(2.37)** in order to determine the normal modal properties and assuming that a solution exists of the form $\{v(t)\} = \{v(\omega)\}e^{i\omega t}$ where $\{v(\omega)\} = \{v\}$ is a vector of time-independent amplitudes, leads to [7]

$$([K] - \omega^2[M])\{v\}e^{i\omega t} = \{0\} \tag{2.38}$$

The eigenvalue problem [10]

$$([K] - \omega_0^2[M])\{Y\} = 0 \tag{2.39}$$

yields p undamped eigenfrequencies where p is the number of degree of freedoms. Substituting any one of these back into the eq. **(2.38)** yields a corresponding set of relative mode shapes $\{Y\}_j$. The complete solution of two (p,p)-eigenmatrices can be expressed as $\left[{\omega_0}_j{}^2\right]_{p,p}$ and $[Y]_{p,p}$ where ${\omega_0}_j{}^2$ is the j_{th}eigenvalue and $\{Y\}_j$ is the corresponding eigenvector. While the eigenvalues are uniquely quantities, the eigenvectors are subject to an indeterminate scaling factor which does not affect the shape of the vibration mode, only its amplitude.

The modal model possesses orthogonality properties

$$[Y]^T[M][Y] = \left[M_g\right] = diag(m_{g1} \dots m_{gj} \dots m_{gp}) \tag{2.40}$$

$$[Y]^T[K][Y] = \left[K_g\right] = diag(k_{g1} \dots k_{gj} \dots k_{gp}) \tag{2.41}$$

$$[{\omega_0}^2] = \left[K_g\right]\left[M_g\right]^{-1} \tag{2.42}$$

where $[M_g]$ and $\left[K_g\right]$are called the diagonal modal or generalized mass and stiffness matrices. Because the eigenvector matrix is subject to an arbitrary scaling factor, the values of $[M_g]$ and $\left[K_g\right]$ are not unique and it is inadvisable to refer to the generalised mass or stiffness of a particular mode. Among the many scaling or normalization processes – the mass-normalization has most relevance to modal testing. The mass-normalized eigenvectors are written as $[\phi]$ and have particular property that [10]

$$[\phi]^T[M][\phi] = [I] \tag{2.43}$$

and thus

$$[\phi]^T[K][\phi] = [{\omega_0}^2] \tag{2.44}$$

The mass-normalized mode shape matrix can be found from

$$[\phi] = [Y]\left[M_g\right]^{-\frac{1}{2}} \tag{2.45}$$

In approaching the more general case of damped systems, it is convenient to consider first a special type of damping called proportional damping which has the advantage of being particularly easy to analyze. In effect, it is possible to derive the modal properties of a proportionally damped system by analyzing in full the undamped version and then making a correction for the presence of the damping.

The definition of proportional damping is [4]

$$[C] = \alpha[K] + \beta[M] \tag{2.46}$$

The damping matrix can be pre- and post-multiplied by the eigenvector matrix for the undamped system $[Y]$

$$[Y]^T[C][Y] = \alpha\left[K_g\right] + \beta\left[M_g\right] = \left[C_g\right] = diag(c_{g1} \dots c_{gj} \dots c_{gp}) \tag{2.47}$$

where $\left[C_g\right]$ is the generalized diagonal damping matrix that represents the generalized damping factors c_{gj} and various modes of the system. Each mode has a complex eigenvalue. The imaginary or oscillatory part is the damped eigenfrequency [10]

$$\omega_{dj} = \omega_{0j}\sqrt{1 - {\zeta_j}^2} \tag{2.48}$$

The real part of the complex eigenvalue represents the decay constant

$$\zeta_j = \frac{c_{gj}}{2\sqrt{k_j m_j}} = \frac{c_{gj}}{2\omega_{0j} m_j} \tag{2.49}$$

The accelerance frequency response function (FRF) of MDOF system is given [10]

$$FRF = [H(\omega)] = \frac{Response}{Excitation}$$

The square and symmetric accelerance FRF matrix describes the relation between the excitation and acceleration response. An element of s^{th} row and k^{th} column amounts to [7]

$$H_{sk}(\omega) = \frac{\ddot{v}_s}{F_{effk}} = \sum_{j=1}^{p} \frac{-\omega^2 Y_{sj} Y_{kj}}{k_j - \omega^2 m_j + i\omega c_j} \tag{2.50}$$

and presents the relation between the excitation on the dof k and the acceleration response on dof s. A dynamical relative acceleration response $\{\ddot{v}\}$ of the MDOF system in the case of pure base excitation $(\{f\} = 0)$ can be rewritten as [7]

$$\{\ddot{v}\} = \sum_{j=1}^{p} \frac{\omega^2 \{Y\}_j {\{Y\}_j}^T ([M][G]\{\ddot{u}_0\})}{k_j - \omega^2 m_j + i\omega c_j} \tag{2.51}$$

3 Identification of System Parameters from Vibration Test Data

The vibration test data of the test structure can be used for the identification of its modal parameters like eigenfrequencies, mode shapes and damping. The test structures can be excited by different types of vibration exciter. Aerospace structures are sometimes investigated on electrohydraulic shaker tables. These exciters significantly interact with the structure under the test [7] and [18]. This interaction or cross-talk results in an unsolicited motion of the shaker table during the test. The consequence is that the frequency response functions (FRFs) cannot be calculated for this interaction frequency range [7]. The influence of the cross-talk has to be considered by the modal identification methods. The following chapter presents such identification method called ISSPA (Identification of Structural System Parameters) that identifies modal parameters without calculating FRFs.

The following chapter consists of two main parts. The first part introduces several typical technical configurations of electrohydraulic shakers. It is shown how to compute the cross-talk frequency range where FRFs cannot be determined. Finally the calculation of the measured base accelerations and relative responses is described. In the second part the identification method ISSPA is in details presented to illustrate the modal identification by means of multi-axis base excitation.

3.1 Vibration Test Environment

For the purpose of modal identification by base excitation, the overall test structure has to be mounted on a shaker table and excited in all spatial degrees of freedom. The multi-axis base acceleration (input) and the structural responses (output) have to be measured. If also the interface forces between the test structure and the shaker table are measured in addition, it is also possible to identify modal and effective mass [6].

The base excitation can be introduced by different types of base exciters. For large aerospace structures it is convenient to use electrohydraulic exciters. In order to measure the structural accelerations, the test structure needs to be equipped with a sufficient number of accelerometers. These accelerometers measure the absolute accelerations. It is shown how to calculate the relative acceleration signals of the accelerometers at the base and at the test structure [6].

3.1.1 Multi-axis base exciter

The multi-axis base exciter like the shaker is an electrohydraulic exciter that is generally used for low frequency excitation environments that require large amounts of force and relatively low velocities. The frequency range varies from near 0 Hz on the low end to 100 Hz on the high end. The parameters and a typical configuration for exciter are given in Table A.1. The multi-axis shaking table is normally used for earthquake simulation and the dynamic qualification of structures. In most cases the same set-up can also be used for the modal identification of the tested structure [6].

3.1.2 Measured base acceleration

For reliable determination of the base acceleration vector $\{\ddot{u}_0\}$, it is required to adequately place a sufficient number of accelerometers at the base of the structure [6]. As example Figure 3.1 shows the typical shaker table with four shaker sensors j. It has to be assumed that there are no elastic deformations during the test $\left(\{\ddot{v}_j\}_{shaker} = 0\right)$ on the shaker. According to eq. **(2.34)** the acceleration of an arbitrary base sensor j_{shaker} in relative system is given by

$$\{\ddot{u}_{j_{shaker}}\} = \{\ddot{u}_b\} + \left[\tilde{\dot{\Omega}}\right] \times \{d_{j_{shaker}}\} \tag{3.1}$$

or according to eq. **(2.34)**

$$\{\ddot{u}_{j_{shaker}}\} = \{\ddot{v}_{j_{shaker}}\} + \{\ddot{u}_b\} + [D_{j_{shaker}}]\{\ddot{\varphi}_b\} \tag{3.2}$$

Expanding eq. **(3.1)** for all base sensors $j_{shaker} = 1,2, \dots p_{shaker}$ gives

$$\begin{Bmatrix} \{\ddot{u}_1\} \\ \vdots \\ \{\ddot{u}_{p_{shaker}}\} \end{Bmatrix} = \begin{bmatrix} [I] & [D_1] \\ \vdots & \vdots \\ [I] & [D_{p_{shaker}}] \end{bmatrix} \begin{Bmatrix} \{\ddot{u}_b\} \\ \{\ddot{\varphi}_b\} \end{Bmatrix} \tag{3.3}$$

or in generally form

$$\{\ddot{u}\}_{shaker} = [G]_{shaker}\{\ddot{u}_0\} \tag{3.4}$$

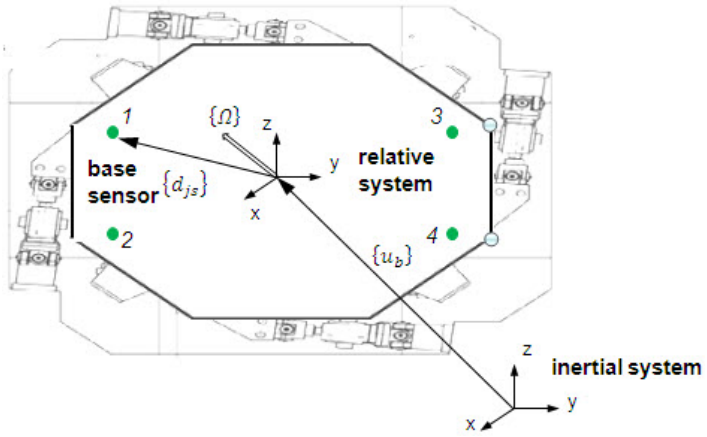

Figure 3.1: Determination of base excitation

The calculation of the six base accelerations $\{\ddot{u}_0\}$ at the base should be performed by using an overdetermined set of equations. Solving the overdetermined set of equations with a least-squares approach reduces the effect of measurement noise signals [7]:

$$\{\ddot{u}_0\} = \left([G]^T_{shaker}[G]_{shaker}\right)^{-1}[G]^T_{shaker}\{\ddot{u}\}_{shaker} \tag{3.5}$$

3.1.3 Measured relative acceleration

The accelerometers on the tested structure measure the absolute accelerations. Therefore, the relative accelerations have to be determined. They can be calculated from measured data by employing rearranged equation **(2.36)**:

$$\{\ddot{v}\} = \{\ddot{u}\}_{struct} - [G]_{struct}\,\{\ddot{u}_0\} \tag{3.6}$$

As this equation contains the previously calculated base accelerations $\{\ddot{u}_0\}$ and the coordinates of the structural accelerometers in matrix$[G]_{struct}$, any inaccuracy of these data results in errors for the relative accelerations [7].

3.1.4 Cross-talk frequency range

To extract the FRF matrix $[H(\omega)]$ it is convenient to drive each base axis by a suitable random or sinusoidal excitation signal. As experience in modal identification testing has shown, a sine sweep is best in most cases [7]. The measured data can then be employed for the determination of the base acceleration input $\{\ddot{u}_0\}$ and the relative acceleration $\{\ddot{v}\}$ of the structure, as outlined above. The input-output relationship can be rewritten in the more general formulation [7]:

$$\{\ddot{v}(\omega)\} = [H(\omega)]\{\ddot{u}_0(\omega)\} \tag{3.7}$$

where $[H(\omega)]$ is a rectangular FRF matrix. If the multi-axis vibration test facility is capable of realizing an excitation precisely in the direction of each base axis, the determination of the FRF matrix $[H(\omega)]$ is straightforward. Driving the translational and rotational axes one after other, the related columns of matrix $[H(\omega)]$ can be determined by simply dividing the relative accelerations $\{\ddot{v}(\omega)\}$ by the acceleration $\ddot{u}(\omega)_{0k}$ of the active base axis. Whenever six linearly independent base accelerations can be realized, the complete FRF matrix can be computed. Inserting measured data into eq.**(3.7)** results in [7]

$$[\{\ddot{v}(\omega)\}_1 \quad \dots \quad \{\ddot{v}(\omega)\}_6] = [H(\omega)][\{\ddot{u}_0(\omega)\}_1 \quad \dots \quad \{\ddot{u}_0(\omega)\}_6] \tag{3.8}$$

or in general form

$$[S_v(\omega)]_{p,6} = [H(\omega)][S_u(\omega)]_{6,6} \tag{3.9}$$

The base acceleration vector $\{\ddot{u}_0(\omega)\}_1$ represents the frequency-domain data from the first test run, and vector $\{\ddot{v}(\omega)\}_1$ comprises the related structural responses. The FRF matrix can then be calculated from

$$[H(\omega)] = [S_v(\omega)][S_u(\omega)]^{-1} \tag{3.10}$$

A requirement for the matrix inversion is the fact that $[S_u(\omega)]$ is regular [7]. Most of the multi-axis vibration test facilities exhibit a more or less strong cross-talk of base axes. This is because the transla-

tional table motions are often coupled with table rotation [18]. In this case the matrix $[S_u(\omega)]$ becomes singular because the six base axes perform linearly dependent motions. The degree of singularity can be checked and visualized by a suitable condition number [7]:

$$c_H = \frac{det[S_u(\omega)]}{\prod_{k=1}^{6} \sqrt{\sum_{l=1}^{6} S_{ukl} S_{ukl}^{*}}} \tag{3.11}$$

Plotting the condition number versus frequency reveals those frequency ranges which are not suitable for further analysis. The FRFs can be computed only for frequency ranges with a high condition number. For that reason the identification method has to be accomplished without using FRFs. It will be shown in the following sections that the identification method ISSPA needs only measured base excitation $\{\ddot{u}_0\}$ and measured relative responses $\{\ddot{v}\}$ data that can be obtained from equations **(3.5)** and **(3.6)**.

3.2 Identification Method

The identification method ISSPA can be applied to vibration test data in order to identify modal parameters [13], [14], [15], [16] and [17]. The ISSPA method needs only measured excitation $\{\ddot{u}_0\}$ and measured relative response data $\{\ddot{v}\}$ that can be inserted into the equation of motion **(2.37)** for base excited MDOF systems in order to extract mass modified stiffness and damping matrices. These system matrices enable the identification of eigenfrequencies, mode shapes and damping.

This section firstly covers how to derive the identification equation from the equation of motion **(2.37)** using incomplete vibration test data. Incomplete data means that the number r of significantly excited modes or effective degrees of freedom is smaller than the number p of the measurement DOF ($r < p$).

In the reality the identification equation have no rank defect matrices ($r = p$). As result ($r - p$) noise eigenvalues will be computed. So the number r of significantly excited modes has to be found. Procedures for rank estimation are presented. Estimated rank r enables to condens the identification equation. The following condensed eigenvalue problem of identified condensed system matrices gives the eigenvalues where the noise eigenvalues are eliminated. The backtransformation to the physical coordinates allows plotting the mode shapes and comparing them with analytical mode shapes. It is also possible to compute the recalculating responses and compare them with the measured responses.

3.2.1 Identification equation

The equation of motion **(2.37)** of a discrete MDOF structure whose danamic behaviour and geometry is assumed to be linear is given by

$$[M]\{\ddot{v}(t)\} + [C]\{\dot{v}(t)\} + [K]\{v(t)\} = \{f(t)\} - [M][G]\{\ddot{u}_0(t)\} = \{F_{eff}(t)\}$$

where $[G] = [G]_{struct}$ is the known time independent geometry matrix of the structure.

Transformation of eq. **(2.37)** into the frequency domain by use of the steady state response solution, in the case of harmonic (sinusoidal) excitation, yields

$$(-\omega^2[M] + i\omega[C] + [K])\{\ddot{v}(i\omega)\} = -\omega^2\{F_{eff}(i\omega)\} \tag{3.12}$$

where $\{F_{eff}(i\omega)\}$ is the effective force vector

$$\{F_{eff}(i\omega)\} = (\{f(i\omega)\} - [M][G]\{\ddot{u}_0(i\omega)\}) \tag{3.13}$$

Premultipying eq. **(3.12)** with the inverse mass matrix $[M]^{-1}$ yields

$$(-\omega^2[I] + i\omega[C^*] + [K^*])\{\ddot{v}(i\omega)\} = -\omega^2([M]^{-1}\{f(i\omega)\} - [I][G]\{\ddot{u}_0(i\omega)\}) \tag{3.14}$$

where

$$[I] = [M]^{-1}[M] \tag{3.15}$$

is the unit matrix,

$$[C^*]_{(p,p)} = [M]^{-1}[C] \tag{3.16}$$

is the mass modified damping matrix and

$$[K^*]_{(p,p)} = [M]^{-1}[K] \tag{3.17}$$

is the mass modified stiffness matrix with p being the number of measured DOF on the test structure.

In the vibration test the amplitude and phase of p measuring points at n_{th} excitation frequency ω_n are calculated from measured data from eq. **(3.6)** and transformed to the real part $\{\ddot{v}\}_{Re}$ and imaginary part $\{\ddot{v}\}_{Im}$ of the complex response

$$\{\ddot{v}(i\omega)\}_n = \{\ddot{v}(\omega)\}_{n,Re} + i\{\ddot{v}(\omega)\}_{n,Im} \qquad (n = 1,2 \dots m) \tag{3.18}$$

where m is the total number of excitation frequencies. Using the measured complex acceleration response **(3.18)** and complex excitation vector $\{F_{eff}(i\omega)\}_n = \{F_{eff}(\omega)\}_{n,Re} + i\{F_{eff}(\omega)\}_{n,Im}$ the following identification equation can be derived by separating eq. **(3.14)** into real and imaginary parts and assembling at ω_n $(n = 1,2 \dots m)$ frequency points:

$$[A][K^*]^T - [\omega][B][C^*]^T + [\omega^2]\{f\}_{Re}[M]^{-1} = [\omega^2][A_u]^T[G]^T_{struct} + [\omega^2][A] \tag{3.19}$$

$$[B][K^*]^T + [\omega][A][C^*]^T + [\omega^2]\{f\}_{Im}[M]^{-1} = [\omega^2][B_u]^T[G]^T_{struct} + [\omega^2][B] \tag{3.20}$$

where

$$[A]_{(m,p)}, [B]_{(m,p)} = \begin{bmatrix} \ddot{v}_1(\omega_1) & \dots & \ddot{v}_j(\omega_1) & \dots & \ddot{v}_p(\omega_1) \\ \vdots & \vdots & \vdots & \vdots & \vdots \\ \ddot{v}_1(\omega_n) & \dots & \ddot{v}_j(\omega_n) & \dots & \ddot{v}_p(\omega_n) \\ \vdots & \vdots & \vdots & \vdots & \vdots \\ \ddot{v}_1(\omega_m) & \dots & \ddot{v}_j(\omega_m) & \dots & \ddot{v}_p(\omega_m) \end{bmatrix}_{Re,Im} \tag{3.21}$$

is (m, p)- measured rectangular real and imaginary part relative acceleration frequency response matrix;

$$[A_u]^T,\ [B_u]^T = \begin{bmatrix} \ddot{u}_{bx}(\omega_1) & \ddot{u}_{by}(\omega_1) & \ddot{u}_{bz}(\omega_1) & \ddot{\varphi}_{bx}(\omega_1) & \ddot{\varphi}_{by}(\omega_1) & \ddot{\varphi}_{bz}(\omega_1) \\ \vdots & \vdots & \vdots & \vdots & \vdots & \vdots \\ \ddot{u}_{bx}(\omega_n) & \ddot{u}_{by}(\omega_n) & \ddot{u}_{bz}(\omega_n) & \ddot{\varphi}_{bx}(\omega_n) & \ddot{\varphi}_{by}(\omega_n) & \ddot{\varphi}_{bz}(\omega_n) \\ \vdots & \vdots & \vdots & \vdots & \vdots & \vdots \\ \ddot{u}_{bx}(\omega_m) & \ddot{u}_{by}(\omega_m) & \ddot{u}_{bz}(\omega_m) & \ddot{\varphi}_{bx}(\omega_m) & \ddot{\varphi}_{by}(\omega_m) & \ddot{\varphi}_{bz}(\omega_m) \end{bmatrix}_{Re,Im} \tag{3.22}$$

is $(m, 6)$- measured real and imaginary part base excitation matrix that can be calculated from eq.**(3.5)**,

$$\{f\}_{Re,Im} = \begin{bmatrix} f(\omega_1)_1 & \dots & f(\omega_1)_j & \dots & f(\omega_1)_p \\ \vdots & \vdots & \vdots & \vdots & \vdots \\ f(\omega_n)_1 & \dots & f(\omega_n)_j & \dots & f(\omega_n)_p \\ \vdots & \vdots & \vdots & \vdots & \vdots \\ f(\omega_m)_1 & \dots & f(\omega_m)_j & \dots & f(\omega_m)_p \end{bmatrix}_{Re,Im} \tag{3.23}$$

is (m, p)- measured force excitation matrix,

$$[\omega] = \begin{bmatrix} \omega_1 & 0 & 0 & 0 & 0 \\ 0 & \ddots & 0 & 0 & 0 \\ 0 & 0 & \omega_n & 0 & 0 \\ 0 & 0 & 0 & \ddots & 0 \\ 0 & 0 & 0 & 0 & \omega_m \end{bmatrix} \tag{3.24}$$

is the (m, m)- diagonal excitation frequency matrix.

From equations **(3.19)** and **(3.20)** it follows that in the case of pure base excitation $(\{f\}_{Re,Im} = 0)$only the mass modified stiffness $[K^*]$ and damping $[C^*]$ matrices can be identified. The result is the following extension of the identification equation

$$[A][K^*]^T - [\omega][B][C^*]^T = [\omega^2][A_u]^T[G]^T_{struct} + [\omega^2][A] \tag{3.25}$$

$$[B][K^*]^T + [\omega][A][C^*]^T = [\omega^2][B_u]^T[G]^T_{struct} + [\omega^2][B] \tag{3.26}$$

or in matrix notation

$$\begin{bmatrix} [A] & -[\omega][B] \\ [B] & [\omega][A] \end{bmatrix} \begin{bmatrix} [K^*]^T \\ [C^*]^T \end{bmatrix} = \begin{bmatrix} ([\omega^2][A_u]^T[G]^T_{struct} + [\omega^2][A]) \\ ([\omega^2][B_u]^T[G]^T_{struct} + [\omega^2][B]) \end{bmatrix} \tag{3.27}$$

3.2.2 Number of effective degrees of freedom

Since the measurements are performed within a given finite frequency range only those eigenmodes with eigenfrequencies lying in this interval have an influence on the structure's response. The number of these eigenmodes is equal to the rank of the response matrices $[A]$ and $[B]$ if all these eigenmodes contribute significantly to the response [15].

The limited number of eigenmodes with eigenfrequencies lying within the measured frequency range and with significant contributions to the response is called the number of effective DOF. This number is equal to the rank r of the response matrices $[A]$ and $[B]$ [15].

3.2.3 Computational eigenvalues

The vibration test will be denoted as incomplete when the number r of excited modes is smaller than the number of measurement degree of freedoms p $(r < p)$. In this case the measurement matrices $[A]$

and $[B]$ theoretically must have the rank $r < p$. However, in practical measurements no rank defect of measured $[A]$ and $[B]$ will be detected because of [16]

- measurement noise,
- the inadequacy of the linearity assumption

Identification equation **(3.27)** that presents then a set of overdetermined equations could now be solved by standard least square procedures with respect to the parameter matrices $[K^*]^T$ and $[C^*]^T$ [16] and [13]. When procedure will be applied to real measurement data severe limitations could be experienced due to the incompleteness of measured data. The consequence is that a complete set of p modes would be calculated from $[K^*]$ and $[C^*]$ including $p - r$ noise or computational modes. In other words the following eigenvalue solution [16]

$$[K^*]\{Y\} = \omega_0^2\{Y\} \tag{3.28}$$

of the identified mass stiffness matrix $[K^*]$ yields the additional undamped $p - r$ noise eigenvalues and $p - r$ eigenvectors. Similarly, the eigenvalue solution of [13]

$$\left\{\lambda\begin{bmatrix}[C^*] & [I]\\ [I] & [0]\end{bmatrix} + \begin{bmatrix}[K^*] & [0]\\ [0] & -[I]\end{bmatrix}\right\}\begin{Bmatrix}\{Y\}\\ \lambda\{Y\}\end{Bmatrix} = \begin{bmatrix}[0]\\ [0]\end{bmatrix} \tag{3.29}$$

yields the additional $p - r$ the damped (complex) noise eigenvalues and $p - r$ eigenvectors. Practical experience revealed that computational and structural modes could not always be separated and influenced each other. Any successful direct matrix identification procedure therefore has to account for the incompleteness condition, i.e. the effect of computational modes has to be extracted from the identification equation, otherwise the method will fail for real world applications [16].

3.2.4 Procedures for rank estimation

In this following subsection two procedures for rank estimation will be described. The method is based on singular value decomposition of measurement matrix $[B]$ ($[A]$ accordingly) [16]:

$$[B]_{(m,p)} = [U_B]_{(m,p)}[S_B]_{p,p}[V_B]^T_{(p,p)} \tag{3.30}$$

where $[U_B]$ represents the modal matrix of $[B][B]^T$, $[V_B]$ represents the modal matrix of $[B]^T[B]$ and $[S_B]$ contains the square of the eigenvalues or singular values of $[B]^T[B]$:

$$[S_B] = diag(s_1 \ \dots \ s_r \ s_{r+1} \ \dots \ s_p) \tag{3.31}$$

Depending on the amount of measurement errors the magnitude errors of the singular values will drop more or less significantly beyond r. A typical curve obtained from measurement data is shown in Figure 3.2 for the ratio s_j/s_{j+1} of consecutive singular values where the rank is indicated by a significant peak of that ratio.

Practical applications revealed that rank determination according to Figure 3.2 was not sufficient to obtain a rank leading to good identification results. Therefore a second procedure was introduced.

With r estimated either from the first step or by number of frequency response peaks the singular value matrix is reduced to [16]

$$[\tilde{S}_B] = diag(s_1 \ \dots \ s_r) \tag{3.32}$$

by artificially setting $s_j = 0$ for $j = r + 1, \dots p$.

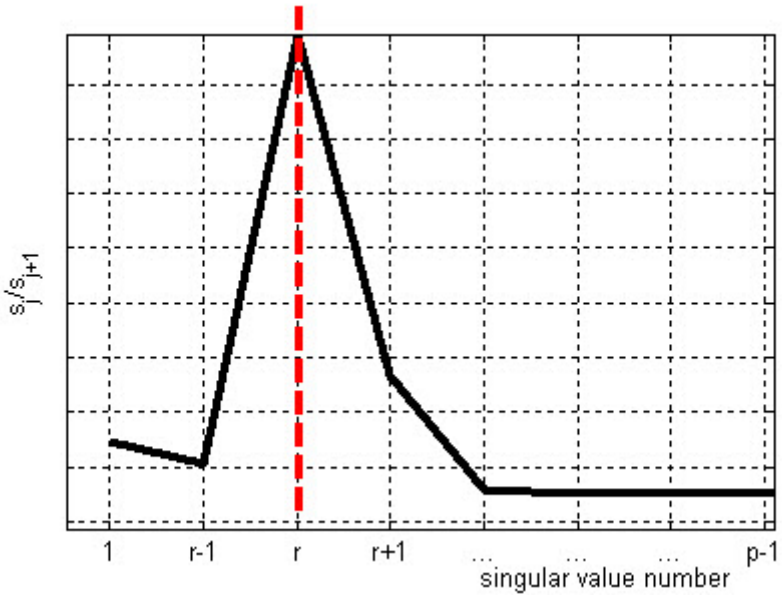

Figure 3.2: Rank estimation

Introducing $[\tilde{S}_B]$ into eq. **(3.69)** instead of $[S_B]$ a modified substitute measuring matrix $[\tilde{B}]$ ($[\tilde{A}]$ accordingly) of rank $r < p$ is obtained:

$$[\tilde{B}] = [\tilde{U}_B][\tilde{S}_B][\tilde{V}_B]^T \tag{3.33}$$

where $[\tilde{U}_B]$ and $[\tilde{V}_B]$ are submatrices of $[U_B]$ and $[V_B]$ belonging to the non-zero values of $[S_B]$.

A numerical criterion for the determination of the effective mode number r is derived from the numerical deviation between the substitute measuring matrices and the original data. The criterion used in ISSPA is the root mean square (rms) error at the j_{th} degree of freedom

$$rms_j = \sqrt{\frac{\sum_n \left(\tilde{B}_{nj} - B_{nj}\right)^2}{\sum_n B_{nj}^2}} \tag{3.34}$$

Practical experience showed that the identification was successful even when the rms_j-deviations were very large at some measurement DOF depending on the magnitude of the signal [16]. Therefore the rms-values of the complete matrix was also used

$$rms = \sqrt{\frac{\sum_n \sum_j \left(\tilde{B}_{nj} - B_{nj}\right)^2}{\sum_n \sum_j B_{nj}^2}} \tag{3.35}$$

where the influence of large errors on small signals is not so pronounced.

The rms-values are equal to zero in the case of ideal measurement data without noise and systematic errors when the singular values beyond r are equal to zero

For real measurement data the rms-values will be non-zero. If plotted versus differently estimated rank numbers r as shown in Figure 3.3, the minimal number required to obtain a reasonable substitute measurement can be derived from the steepest change of slope of that curve [16].

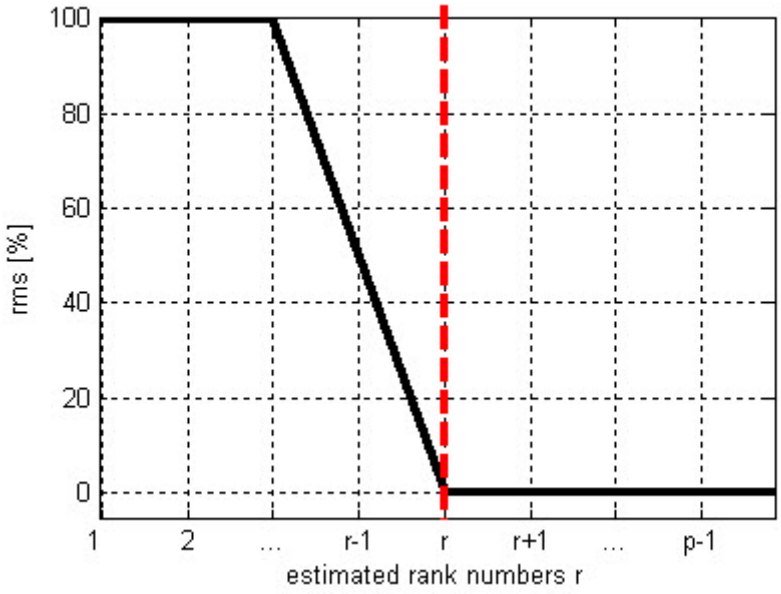

Figure 3.3: rms-deviation of substitute measurement rank of measurement matrix

3.2.5 Condensed identification equation

The measurement matrices $[A]$ and $[B]$ of rank p in eq. **(3.27)** should be replaced by substitute measurement matrices $[\tilde{A}]$ and $[\tilde{B}]$ of estimated rank r [15]. These matrices are incomplete because the influence of the higher modes is eliminated [13]. It is essential to introduce the following properties of pseudo-unit matrices for the substitute measurement matrices $[\tilde{A}]$ and $[\tilde{B}]$ [13]:

$$[\tilde{I}] = [\tilde{A}]^+[\tilde{A}] = [\tilde{B}]^+[\tilde{B}] = [\tilde{V}_A][\tilde{V}_A]^T = [\tilde{V}_B][\tilde{V}_B]^T \tag{3.36}$$

The pseudo-unit matrix $[\tilde{I}]$ has the rank r and the properties:

$$[\tilde{A}] = [\tilde{A}][\tilde{I}] = [\tilde{A}][\tilde{V}_B][\tilde{V}_B]^T \tag{3.37}$$

and

$$[\tilde{B}] = [\tilde{B}][\tilde{I}] = [\tilde{B}][\tilde{V}_A][\tilde{V}_A]^T \tag{3.38}$$

The substitute measurement matrices can now be transformed to r principal coordinates by the (p,r)-transformation matrix $[\tilde{V}] = [\tilde{V}_B]$. Introducing the properties **(3.37)** and **(3.69)** into eq. **(3.27)** and right-multiplying by the transformation matrix $[\tilde{V}]$ leads to a condensed regular identification equation [13]:

$$\begin{bmatrix} [\hat{A}] & -[\omega][\hat{B}] \\ [\hat{B}] & [\omega][\hat{A}] \end{bmatrix} \begin{bmatrix} [\hat{K}^*]^T \\ [\hat{C}^*]^T \end{bmatrix} = \begin{bmatrix} ([\omega^2][A_u]^T[G]^T_{struct}[\tilde{V}] + [\omega^2][\hat{A}]) \\ ([\omega^2][B_u]^T[G]^T_{struct}[\tilde{V}] + [\omega^2][\hat{B}]) \end{bmatrix} \tag{3.39}$$

where

$$[\hat{A}]_{m,r} = [\tilde{A}]_{m,p}[\tilde{V}]_{p,r} \tag{3.40}$$

and

$$[\hat{B}]_{m,r} = [\tilde{B}]_{m,p}[\tilde{V}]_{p,r} \tag{3.41}$$

with respect to the condensed parameter matrices

$$[\hat{K}^*]_{(r,r)} = [\tilde{V}]^T[K^*]_{(p,p)}[\tilde{V}] \tag{3.42}$$

and

$$[\hat{C}^*]_{(r,r)} = [\tilde{V}]^T[C^*]_{(p,p)}[\tilde{V}] \tag{3.43}$$

that can be calculated by the least square procedures [13].

3.2.6 Determination of the real modal data from condensed matrices

Solving the condensed right undamped eigenvalue [13]

$$[\hat{K}^*]\{\hat{Y}\} = \omega_0^2\{\hat{Y}\} \tag{3.44}$$

yields the r angular eigenfrequencies ω_0 and r condensed eigenmodes $\{\hat{Y}\}$ of the undamped test structure (real data) within measured frequency range.

Solving the condensed left eigenvalue problem

$$\left[\hat{K}^*\right]^T \{\hat{X}\} = \omega_0^2 \{\hat{X}\} \tag{3.45}$$

yields r unnormalized condensed left eigenmodes $\{\hat{X}\}$. The condensed right hand matrix $[\hat{Y}]$ and condensed unnormalized left matrix $[\hat{X}]$ in the principal coordinates can be back transformed to the measured physical coordinates by premultiplying with the transformation matrix$[\tilde{V}]$ [13]:

$$[Y]_{(p,r)} = [\tilde{V}]_{(p,r)} [\hat{Y}]_{(r,r)} \tag{3.46}$$

$$[X]_{(p,r)} = [\tilde{V}]_{(p,r)} [\hat{X}]_{(r,r)} \tag{3.47}$$

3.2.7 Determination of the complex modal data from condensed matrices

In the case of pure base excitation, i.e. $\{f(i\omega)\} = 0$, it is also possible to use the extended eigenvalue solution **(3.29)** in principal coordinates [13]:

$$\{\lambda[E] + [F]\} \begin{Bmatrix} \{\hat{Y}\} \\ \lambda\{\hat{Y}\} \end{Bmatrix} = \begin{bmatrix} [0] \\ [0] \end{bmatrix} \tag{3.48}$$

where

$$[E] = \begin{bmatrix} \left[\hat{C}^*\right] & [I] \\ [I] & [0] \end{bmatrix} \tag{3.49}$$

and

$$[F] = \begin{bmatrix} \left[\hat{K}^*\right] & [0] \\ [0] & -[I] \end{bmatrix} \tag{3.50}$$

Eq. **(3.48)** yields $j = 1, \ldots r$ complex eigenvalues

$$\lambda_j = \lambda_{Re,j} + \lambda_{Im,j} \tag{3.51}$$

with corresponding complex eigenvectors $[\tilde{Y}]_{r,r}$ and r conjugate complex eigenvalues

$$\lambda_j^* = \lambda_{Re,j} - \lambda_{Im,j} \tag{3.52}$$

with corresponding conjugate complex eigenvectors $\left[\hat{Y}^*\right]_{r,r}$.

Any complex eigenvalue λ_j can be expressed as [13]

$$\lambda_j = -\zeta_j \omega_{0j} + i\omega_{0j}\sqrt{1-\zeta_j^2} \tag{3.53}$$

The real part of λ_j, calling decay constant or damping coefficient δ_j, is the negative product of damping ζ_j and eigenfrequencyω_{0j}

$$\lambda_{Re,j} = \delta_j = -\zeta_j \omega_{0j} \tag{3.54}$$

The imaginary part of λ_j is equal to damped eigenfrequency ω_{dj}

$$\lambda_{Im,j} = \omega_{dj} = \sqrt{\omega_{0j}^2 - p_{Re,j}} = \omega_{0j}\sqrt{1-\zeta_j^2} \tag{3.55}$$

The angular eigenfrequency ω_{0j} can be written as

$$\omega_{0j} = \sqrt{\lambda_{Re,j}^2 + \lambda_{Im,j}^2} \tag{3.56}$$

The eigenfrequency is given by

$$f_j = \frac{\omega_{0j}}{2\pi} \tag{3.57}$$

Substituting equations **(3.56)** and **(3.55)** into **(3.54)** gives the damping

$$\zeta_j = \frac{|\lambda_{Re,j}|}{\sqrt{\lambda_{Re,j}^2 + \lambda_{Im,j}^2}} \tag{3.58}$$

3.2.8 Condensed generalized equation of motion

Since left and right condensed eigenvectors are orthogonal, the relation

$$[\hat{Y}]^T[\hat{X}] = [\hat{X}]^T[\hat{Y}] = [\bar{M}_g] = diag(\bar{m}_{g1} \dots \bar{m}_{gr \le gp}) \tag{3.59}$$

holds [13]. Since $[Y]$ and $[X]$, may be normalized arbitrarily, the matrix $[\bar{M}_g]$ is not identical with the generalized matrix $[M_g]$ which follows from eq. **(2.40)**

$$[Y]^T[M][Y] = [M_g] = diag(m_{g1} \dots m_{gr \le gp})$$

The matrices $[\bar{M}_g]$ and $[M_g]$ can be made equal my normalizing the left eigenvectors $[X]$ by a diagonal matrix $[\kappa]$:

$$\left[M_g\right]_{(r,r)} = \left[\bar{M}_g\right][\kappa] = [Y]^T[X][\kappa] = [\hat{Y}]^T[\hat{X}][\kappa] \tag{3.60}$$

But in the case of pure base excitation it is not possible to calculate the κ factors [14].

The generalized damping matrix follows from

$$\left[\bar{C}_g\right]_{(r,r)} = [\hat{X}]^T\left[\hat{C}^*\right][\hat{Y}] \tag{3.61}$$

The generalized damping matrix $\left[\bar{C}_g\right]$ is neither symmetric nor diagonal. The off-diagonal elements represent the coupling of the generalized DOF.

Generalized condensed equation of motion in the case of pure base excitation can be obtained by using the modal transformation in principal coordinates:

$$\left\{\hat{\bar{v}}\right\}_n = [\hat{Y}]\left\{\hat{\bar{q}}\right\}_n \tag{3.62}$$

and premultiplying eq. **(3.14)** with the condensed left modal matrix $\left[\hat{X}\right]^T$

$$\left(-\omega_n^2\left[\bar{M}_g\right] + i\omega_n\left[\bar{C}_g\right] + \left[\bar{M}_g\right][\omega_0^2]\right)\{\ddot{q}(i\omega)\}_n = \omega_n^2[\bar{X}_z]^T[G]_{struct}\{\ddot{u}_0(i\omega)\}_n \tag{3.63}$$

where $[\omega_0^2]$ is the diagonal matrix of the eigenfrequencies. Eq. **(3.63)** is decoupled with respect to the eigenmodes only in case $\left[\bar{C}_g\right] = diag\left(\bar{c}_{gjj}\right)$ [17].

3.2.9 Recalculating responses

In order to check the eigenfrequencies, the eigenmodes and damping matrices these data can be used to calculate the dynamic response and compare it with the original measured response. The agreement between these responses is regarded as a measure for the accuracy of extracted data [17].

The generalized response vector $\{\ddot{q}(i\omega)\}_i$ for the excitation frequency ω_i is obtained from eq. **(3.63)**. Splitting of eq. **(3.63)** into real and imaginary parts yields in the general case $\left[\bar{C}_g\right] \neq diag\left(\bar{c}_{jj}\right)$

$$\begin{bmatrix} [a]_n & -\omega_n\left[\bar{C}_g\right] \\ \omega_n\left[\bar{C}_g\right] & [a]_n \end{bmatrix}\begin{Bmatrix}\{\ddot{q}\}_{Re,n} \\ \{\ddot{q}\}_{Im,n}\end{Bmatrix} = \begin{Bmatrix}\omega_n^2[\bar{X}_z]^T[G]_{struct}\{\ddot{u}_0(i\omega)\}_{Re,n} \\ \omega_n^2[\bar{X}_z]^T[G]_{struct}\{\ddot{u}_0(i\omega)\}_{Im,n}\end{Bmatrix} \tag{3.64}$$

where the diagonal matrix

$$[a]_n = \left(-\omega_i^2[I] + [\omega_0^2]\right)\left[\bar{M}_g\right] \tag{3.65}$$

The real and imaginary parts of the condensed dynamic response in principal coordinates follow from eq. **(3.62)**:

$$\{\hat{\ddot{v}}\}_{Re,n} = [\hat{Y}]\{\hat{\ddot{q}}\}_{Re,n} \tag{3.66}$$

$$\{\hat{\ddot{v}}\}_{Im,n} = [\hat{Y}]\{\hat{\ddot{q}}\}_{Im,n} \tag{3.67}$$

The back transformation to the physical coordinates follows by premultiplying with the transformation matrix $[\tilde{V}]$:

$$\{\ddot{v}\}_{Re,n} = [\tilde{V}]_{(p,r)}\{\hat{\ddot{v}}\}_{Re,n} \tag{3.68}$$

$$\{\ddot{v}\}_{Im,n} = [\tilde{V}]_{(p,r)}\{\hat{\ddot{v}}\}_{Im,n} \tag{3.69}$$

4 Demo Structure

Prior to applying the ISSPA method to complex base-excited structures it is necessary to test it on simpler model or demo structure [20].

This chapter is firstly devoted to the derivation of the reduced system matrices of such simplified MDOF demo structure that consists of three-dimensional (3D) beam elements. When the 3D elements are assembled to the entire demo structure, the number of redundant DOF has to be eliminated. A popular method of reduction of the size of redundant DOF - the Static Condensation Method applied to dynamic problems - is introduced. Also it is offered to considering the inertial properties for a dynamic system because of lumped mass. The procedures of reducing the system matrices are implemented into the MATLAB-function *demostructure.m*.

The second part of this chapter is focused on the multi-axis base excitation simulation of the demo structure. The reduced generalized system matrices, geometry matrix and base excitation vector in eq. **(2.51)** enable to calculate the relative acceleration responses. It will be possible to analyze the influence of the cross-talk effects. The MATLAB-function *response_analysis.m* is programmed for these goals.

4.1 Characteristics of the Demo Structure

The 3D demo structure is taken from [1]. The 3D demo structure consists of four rectangular blades of different lengths mounted perpendicularly on a hollow central mast (Figure 4.1). The overall height is about *1.6 m* and the total mass amounts to about *191 kg*. The sizes and distribution of weight, stiffness and damping are summarized in the Table B.1.

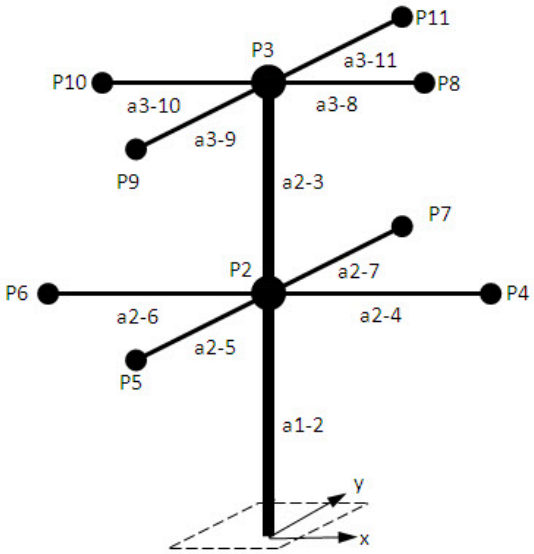

Figure 4.1: Three-dimensional test structure

4.2 Finite-Element Description

The finite-element method (FEM) is an effective numerical method that is used to provide approximations to solutions of static and dynamic problems for continuous systems. Application of the finite-element method requires the system to be divided into a finite number of elements [8].

4.2.1 Local matrices

In this case it is assumed that the demo structure already consists of separate elements. These are 3D beam elements as shown in Figure 4.2 which resist axial force, transverse shear force in each of two directions, bending about each principal axis of the cross section, and torque about longitudinal axis member. Following [3] they contain stiffness qualities of truss-, torsion- and beam elements. Truss elements are hinged at connection points and resist only axial force; torsion moments resist axial moments and beam elements are welded together at connection points and resist transverse forces and bending moments.

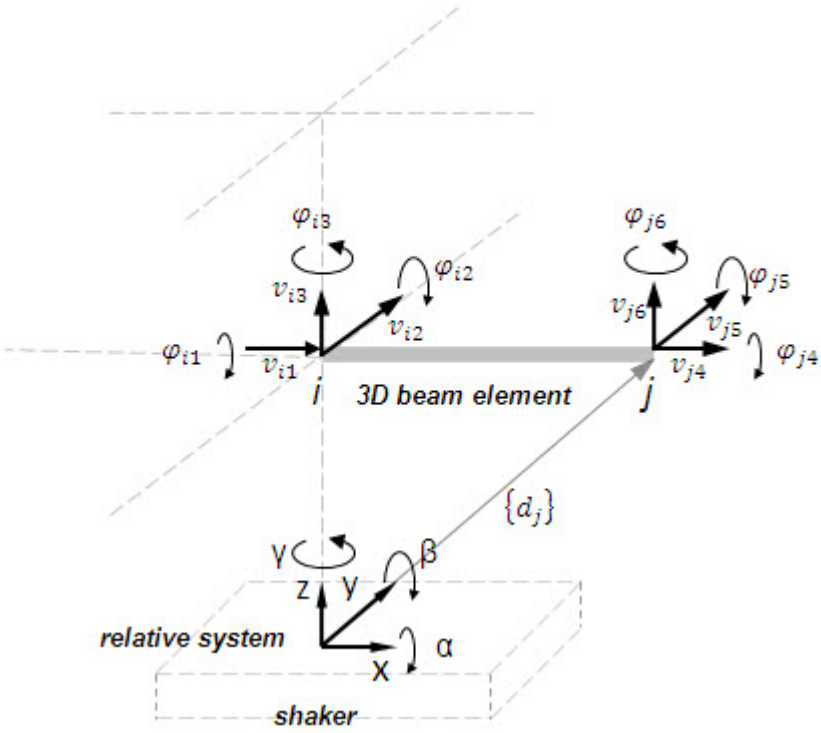

Figure 4.2: 3D beam element: DOF

The effective local force vector acting on nodal points i and j of the 3D beam element contains the difference between external loads and d'Alembert's inertia forces because of the base excitation

$$\{\tilde{F}_{eff}\} = \{\tilde{f}\} - [\tilde{M}][\tilde{G}]\begin{Bmatrix}\{\ddot{u}_b\}\\ \{\ddot{\varphi}_b\}\end{Bmatrix} \tag{4.1}$$

where $\{\tilde{f}\}$ is the local external loads vector as shown in Figure 4.3

$$\{\tilde{f}\} = \{S_{i1}\ S_{i2}\ S_{i3}\ M_{i1}\ M_{i2}\ M_{i3}\ S_{j4}\ S_{j5}\ S_{j6}\ M_{j4}\ M_{j5}\ M_{j6}\}^T \tag{4.2}$$

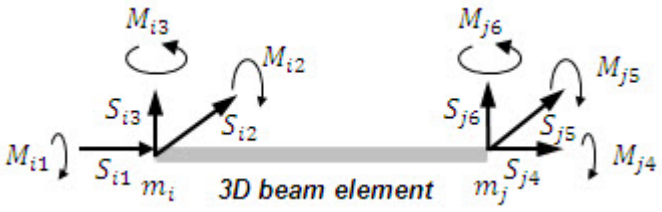

Figure 4.3: 3D external loads

and $[\widetilde{M}]$ is the local lumped mass matrix. The simplest method for considering the inertial properties of the demo structure is to assume that the mass of the structure is lumped at the nodal coordinates as shown in Figure 4.1. The inertial effect associated with any rotational degree of freedom is then assumed to be zero [19]. The local lumped mass matrix $[\widetilde{M}]$ is:

$$[\widetilde{M}] = \begin{bmatrix} m_i & 0 & 0 & 0 & 0 & 0 & 0 & 0 & 0 & 0 & 0 & 0 \\ 0 & m_i & 0 & 0 & 0 & 0 & 0 & 0 & 0 & 0 & 0 & 0 \\ 0 & 0 & m_i & 0 & 0 & 0 & 0 & 0 & 0 & 0 & 0 & 0 \\ 0 & 0 & 0 & 0 & 0 & 0 & 0 & 0 & 0 & 0 & 0 & 0 \\ 0 & 0 & 0 & 0 & 0 & 0 & 0 & 0 & 0 & 0 & 0 & 0 \\ 0 & 0 & 0 & 0 & 0 & 0 & 0 & 0 & 0 & 0 & 0 & 0 \\ 0 & 0 & 0 & 0 & 0 & 0 & m_j & 0 & 0 & 0 & 0 & 0 \\ 0 & 0 & 0 & 0 & 0 & 0 & 0 & m_j & 0 & 0 & 0 & 0 \\ 0 & 0 & 0 & 0 & 0 & 0 & 0 & 0 & m_j & 0 & 0 & 0 \\ 0 & 0 & 0 & 0 & 0 & 0 & 0 & 0 & 0 & 0 & 0 & 0 \\ 0 & 0 & 0 & 0 & 0 & 0 & 0 & 0 & 0 & 0 & 0 & 0 \\ 0 & 0 & 0 & 0 & 0 & 0 & 0 & 0 & 0 & 0 & 0 & 0 \end{bmatrix} \tag{4.3}$$

The local time independent geometry matrix $[\tilde{G}]$ has the following form:

$$[\tilde{G}] = \begin{bmatrix} [I] & [D_i] \\ [0] & [0] \\ [I] & [D_j] \\ [0] & [0] \end{bmatrix} \tag{4.4}$$

where $[D_i]$ and $[D_j]$ are given in eq. **(2.30)**:

$$[D_j] = \begin{bmatrix} 0 & d_{jz} & -d_{jy} \\ -d_{jz} & 0 & d_{jx} \\ d_{jy} & -d_{jx} & 0 \end{bmatrix}$$

One has

$$\{\tilde{F}_{eff}\} = [\widetilde{K}]\{\tilde{v}\} + [\widetilde{M}]\{\ddot{\tilde{v}}\} \tag{4.5}$$

where $\{\tilde{v}\}$ contains the displacements and rotations of the structural nodal points i and j

$$\{\tilde{v}\} = \{v_{i1}\ v_{i2}\ v_{i3}\ \varphi_{i1}\ \varphi_{i2}\ \varphi_{i3}\ v_{j4}\ v_{j5}\ v_{j6}\ \varphi_{j4}\ \varphi_{j5}\ \varphi_{j6}\}^T \tag{4.6}$$

and $[\widetilde{K}]$ is the element stiffness matrix of the 3D beam element. The element stiffness matrix is given by [5]:

$$[\tilde{K}] = \begin{bmatrix}
\frac{EA}{L} & 0 & 0 & 0 & 0 & 0 & -\frac{EA}{L} & 0 & 0 & 0 & 0 & 0 \\
0 & \frac{12EI_z}{L^3} & 0 & 0 & 0 & \frac{6EI_z}{L^2} & 0 & -\frac{12EI_z}{L^3} & 0 & 0 & 0 & \frac{6EI_z}{L^2} \\
0 & 0 & \frac{12EI_y}{L^3} & 0 & -\frac{6EI_y}{L^2} & 0 & 0 & 0 & -\frac{12EI_y}{L^3} & 0 & -\frac{6EI_y}{L^2} & 0 \\
0 & 0 & 0 & \frac{GI_x}{L} & 0 & 0 & 0 & 0 & 0 & -\frac{GI_x}{L} & 0 & 0 \\
0 & 0 & -\frac{6EI_y}{L^2} & 0 & \frac{4EI_y}{L} & 0 & 0 & 0 & \frac{6EI_y}{L^2} & 0 & \frac{2EI_y}{L} & 0 \\
0 & \frac{6EI_z}{L^2} & 0 & 0 & 0 & \frac{4EI_z}{L} & 0 & -\frac{6EI_z}{L^2} & 0 & 0 & 0 & \frac{2EI_z}{L} \\
-\frac{EA}{L} & 0 & 0 & 0 & 0 & 0 & \frac{EA}{L} & 0 & 0 & 0 & 0 & 0 \\
0 & -\frac{12EI_z}{L^3} & 0 & 0 & 0 & -\frac{6EI_z}{L^2} & 0 & \frac{12EI_z}{L^3} & 0 & 0 & 0 & -\frac{6EI_z}{L^2} \\
0 & 0 & -\frac{12EI_y}{L^3} & 0 & \frac{6EI_y}{L^2} & 0 & 0 & 0 & \frac{12EI_y}{L^3} & 0 & \frac{6EI_y}{L^2} & 0 \\
0 & 0 & 0 & -\frac{GI_x}{L} & 0 & 0 & 0 & 0 & 0 & \frac{GI_x}{L} & 0 & 0 \\
0 & 0 & -\frac{6EI_y}{L^2} & 0 & \frac{2EI_y}{L} & 0 & 0 & 0 & \frac{6EI_y}{L^2} & 0 & \frac{4EI_y}{L} & 0 \\
0 & \frac{6EI_z}{L^2} & 0 & 0 & 0 & \frac{2EI_z}{L} & 0 & -\frac{6EI_z}{L^2} & 0 & 0 & 0 & \frac{4EI_z}{L}
\end{bmatrix} \tag{4.7}$$

where E is a modulus of elasticity, G is a shear modulus and L is a length of 3D beam element

4.2.2 Global matrices

The assembly of global stiffness and mass matrices requires that each of the element stiffness equation be referred to the global axes. The geometric transformation contains a rotation through the angles α, β and γ as shown in Figure 4.2. The corresponding transformation is given in [5] as

$$[T] = \begin{bmatrix} [\tilde{T}] & [0] & [0] & [0] \\ [0] & [\tilde{T}] & [0] & [0] \\ [0] & [0] & [\tilde{T}] & [0] \\ [0] & [0] & [0] & [\tilde{T}] \end{bmatrix} \tag{4.8}$$

where

$$[\tilde{T}] = \begin{bmatrix} \cos\beta\cos\gamma & \cos\beta\sin\gamma & -\sin\beta \\ \sin\alpha\sin\beta\cos\gamma - \cos\alpha\sin\beta & \sin\alpha\sin\beta\sin\beta + \cos\alpha\cos\gamma & \sin\alpha\cos\beta \\ \cos\alpha\sin\beta\cos\gamma + \sin\alpha\sin\gamma & \cos\alpha\sin\beta\sin\gamma - \sin\alpha\cos\gamma & \cos\alpha\cos\beta \end{bmatrix} \tag{4.9}$$

The element stiffness matrix $[\tilde{K}]$ and local mass Matrix $[\tilde{M}]$ are transformed to the global coordinates by

$$\left[\widetilde{K}_{3D}\right] = [T]^T\left[\widetilde{K}\right][T] \tag{4.10}$$

$$\left[\widetilde{M}_{3D}\right] = [T]^T\left[\widetilde{M}\right][T] \tag{4.11}$$

The transformed local mass $\left[\widetilde{M}_{3D}\right]$ and stiffness matrices $\left[\widetilde{K}_{3D}\right]$ are assembled into global matrices. After the elimination of the fixed degrees of freedom according to the support the global system matrices $\left[K_{global}\right]$ and $\left[M_{global}\right]$ get the dimension $p, p = 60{,}60$.

4.2.3 Static Condensation

In the case of pure base excitation the eq. **(4.5)** becomes the following form:

$$-[\widetilde{M}]\begin{bmatrix} 1 & 0 & 0 & 0 & d_{jz} & -d_{jy} \\ 0 & 1 & 0 & -d_{jz} & 0 & d_{jx} \\ 0 & 0 & 1 & d_{jy} & -d_{jx} & 0 \\ 0 & 0 & 0 & 0 & 0 & 0 \\ 0 & 0 & 0 & 0 & 0 & 0 \\ 0 & 0 & 0 & 0 & 0 & 0 \\ 1 & 0 & 0 & 0 & d_{jz} & -d_{jy} \\ 0 & 1 & 0 & -d_{jz} & 0 & d_{jx} \\ 0 & 0 & 1 & d_{jy} & -d_{jx} & 0 \\ 0 & 0 & 0 & 0 & 0 & 0 \\ 0 & 0 & 0 & 0 & 0 & 0 \\ 0 & 0 & 0 & 0 & 0 & 0 \end{bmatrix}\begin{Bmatrix} \ddot{u}_{bx} \\ \ddot{u}_{by} \\ \ddot{u}_{bz} \\ \ddot{\varphi}_{bx} \\ \ddot{\varphi}_{by} \\ \ddot{\varphi}_{bz} \end{Bmatrix} = \left[\widetilde{K}\right]\begin{Bmatrix} v_{i1} \\ v_{i2} \\ v_{i3} \\ \varphi_{i1} \\ \varphi_{i2} \\ \varphi_{i3} \\ v_{j4} \\ v_{j5} \\ \varphi_{j4} \\ \varphi_{j5} \\ \varphi_{j6} \end{Bmatrix} + [\widetilde{M}]\begin{Bmatrix} v_{i1} \\ v_{i2} \\ v_{i3} \\ \varphi_{i1} \\ \varphi_{i2} \\ \varphi_{i3} \\ v_{j4} \\ v_{j5} \\ \varphi_{j4} \\ \varphi_{j5} \\ \varphi_{j6} \end{Bmatrix} \tag{4.12}$$

The lumped mass matrix structure results in a diagonal mass matrix and contains zeros in its main diagonal due to assumed zero rotational inertial moments. The local geometry matrix also contains zeros corresponding to rotational degrees of freedom $\varphi_i$and φ_j. These facts enable the elimination by static condensation of the rotational degrees of freedom thus reducing the dimension of the dynamic problem [19].

A practical method of accomplishing the reduction of the stiffness matrix is to identify those degrees of freedom to be condensed as dependent or secondary degrees of freedom and express them in the term of the remaining independent or primary degrees of freedom [9], [19]. In this case the translational degrees of freedom should be condensed and rotational must be eliminated. The stiffness equation for the test structure may be written as

$$\begin{bmatrix} [K_{ss}] & [K_{sp}] \\ [K_{ps}] & [K_{pp}] \end{bmatrix}\begin{Bmatrix} \{\varphi_s\} \\ \{v_p\} \end{Bmatrix} = \begin{Bmatrix} \{0\} \\ \{F_p\} \end{Bmatrix} \tag{4.13}$$

where $\{\varphi_s\}$ is the rotational vector corresponding to the s degrees of freedom to be reduced and $\{v_p\}$ is the displacement vector corresponding to the remaining p independent degrees of freedom. It is assumed that the external forces were zero at the dependent degrees of freedom. A multiplication of the matrices on the left side of eq. **(4.13)** expands this equation into two matrix equations

$$[K_{ss}]\{\varphi_s\} + [K_{sp}]\{v_p\} = \{0\} \tag{4.14}$$

$$[K_{ps}]\{\varphi_s\} + [K_{pp}]\{v_p\} = \{F_p\} \tag{4.15}$$

Equation **(4.14)** is equivalent to

$$\{\varphi_s\} = [\tilde{T}_{sc}]\{v_p\} \tag{4.16}$$

where $[\tilde{T}_{sc}]$ is the transformation matrix given by

$$[\tilde{T}_{sc}] = -[K_{ss}]^{-1}[K_{sp}] \tag{4.17}$$

Substituting eq. **(4.16**) and using eq. **(4.17**) in eq. **(4.15)** results in the reduced stiffness equation relating forces and displacements at the primary coordinates

$$[K]\{v_p\} = \{F_p\} \tag{4.18}$$

where $[K]$ is the reduced stiffness matrix given by

$$[K] = [K_{pp}] - [K_{ps}][K_{ss}]^{-1}[K_{sp}] \tag{4.19}$$

The static relationship between the secondary coordinates $\{\varphi_s\}$ and primary coordinates $\{v_p\}$ may be written using the identity $\{v_p\} = [I]\{v_p\}$ as

$$\begin{Bmatrix}\{\varphi_s\}\\ \{v_p\}\end{Bmatrix} = \begin{Bmatrix}[\tilde{T}_{sc}]\\ [I]\end{Bmatrix}\{v_p\} \tag{4.20}$$

With

$$[T_{sc}] = \begin{bmatrix}[\tilde{T}_{sc}]\\ [I]\end{bmatrix} \tag{4.21}$$

the reduced stiffness matrix can be written as

$$[K] = [T_{sc}]^T[K_{global}][T_{sc}] \tag{4.22}$$

4.2.4 Static Condensation Applied to Dynamic Problems

In order to reduce the mass matrix, it is assumed that the same static relationship between secondary and primary degrees of freedom remains valid in the dynamic problem [2]. Hence the same transformation based on static condensation for the reduction of the global stiffness matrix is also used for reducing the global mass matrix. In general this method of reducing the dynamic problem is not exact.

In this case the discretization of the mass results in a number of massless rotational degrees of freedom selected to be condensed. Thus it is only necessary to carry out the static condensation of the global stiffness matrix and to delete from the global mass matrix the rows and columns corresponding to the massless rotational degrees of freedom.

The static Condensation Method in this case does not alter the original problem, and thus results in an equivalent eigenproblem without introducing any error. In the general case involving the condensation of degrees of freedom to which the discretization process has allocated mass, the reduced mass is obtained using transformations analogues to eq.**(4.22)**

$$[M] = [T_{sc}]^T [M_{global}][T_{sc}] \tag{4.23}$$

The theory presented in aforementioned sections was implemented with MATLAB (*demostructure.m)* in order to get the reduced system matrices $[K]$ and $[M]$ of the demo structure. The Figure 4.4 summarizes the all steps of the derivation of reduced system matrices in the *demostructure.m*.

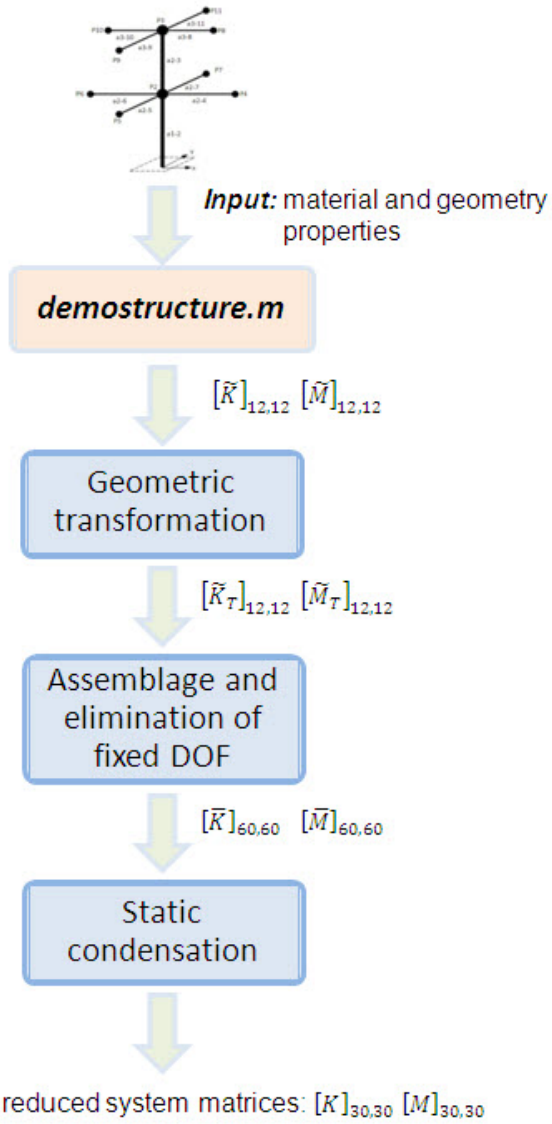

Figure 4.4: Procedures of the reduction of the system matrices of the demo structure

4.3 Response Analysis

The response analysis was implemented with the programmed Matlab-function *response_analysis.m* that accomplishes the eigenvalue problem of the demo structure, plots the mode shapes and simulates the unsolicited motions of the shaker. The input parameters as shown in Figure 4.5 are the reduced system matrices of the demo structure that were derived in the aforementioned sections. The reduced system matrices of the demo structure are used in the eigenvalue solution eq. **(2.38)**

$$([K] - \omega^2[M])\{v\}e^{i\omega t} = \{0\}$$

that yields as output parameters the eigenfrequencies f and eigenvectors $\{Y\}$. Additional function plots the mode shapes of the demo structure. Manipulating of the base excitation vector $\{\ddot{u}_0\}$ allows simulating the base excitation and investigating corresponding responses of virtual sensors (DOF).

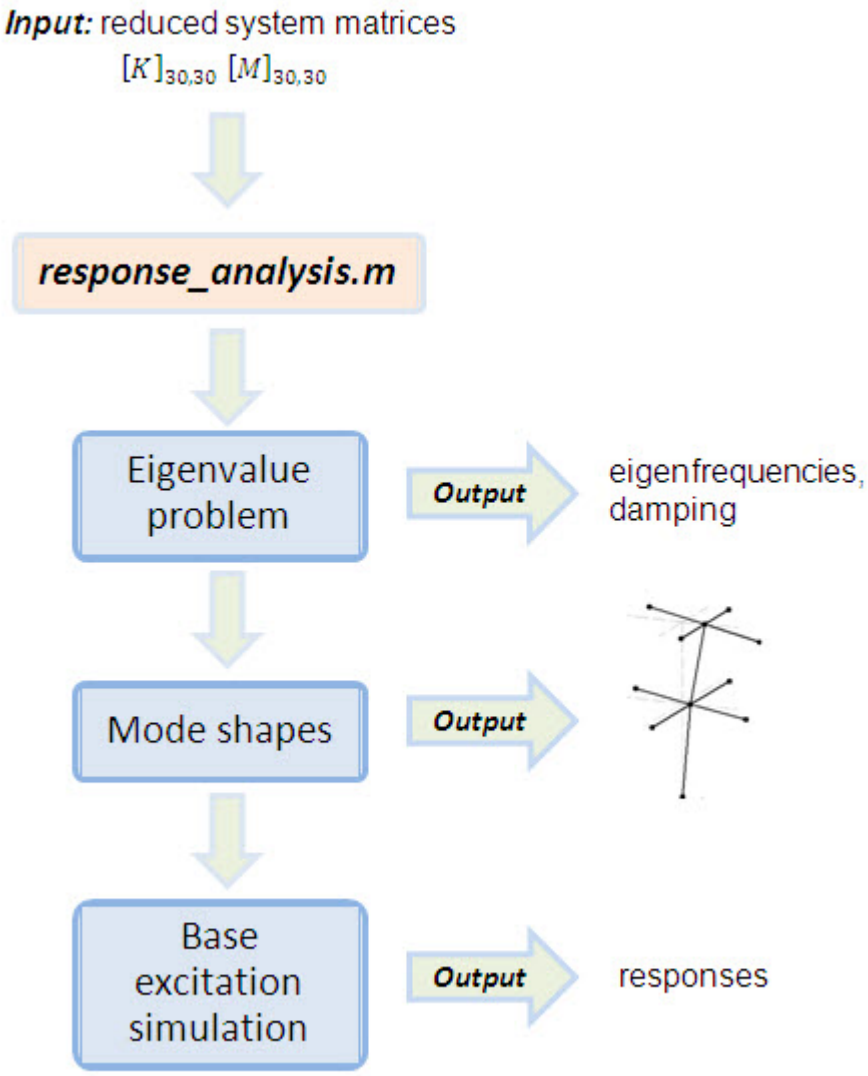

Figure 4.5: Input and output data of the *response_analysis.m*

4.3.1 Eigenvalues of the demo structure

The reduced system matrices $[K]_{30,30}$ and $[M]_{30,30}$ have the dimension $p, p = 30{,}30$ so that 30 eigenfrequencies and mode shapes can be found (Table B.2). There are 16 eigenfrequencies up to 100 Hz. The lowest eigenfrequency is $f_1 = 9{,}37Hz$. The corresponding mode shape is a pendulum motion of the central mast about its x-axis as shown in Figure 4.6. The corresponding mode shape to the second eigenfrequency $f_2 = 11{,}86\ Hz$ contains the pendulum motion of the central mast about its y-axis. The corresponding mode shape to the third eigenfrequency $f_3 = 12{,}01\ Hz$ contains the oscillating motion about its z-axis.

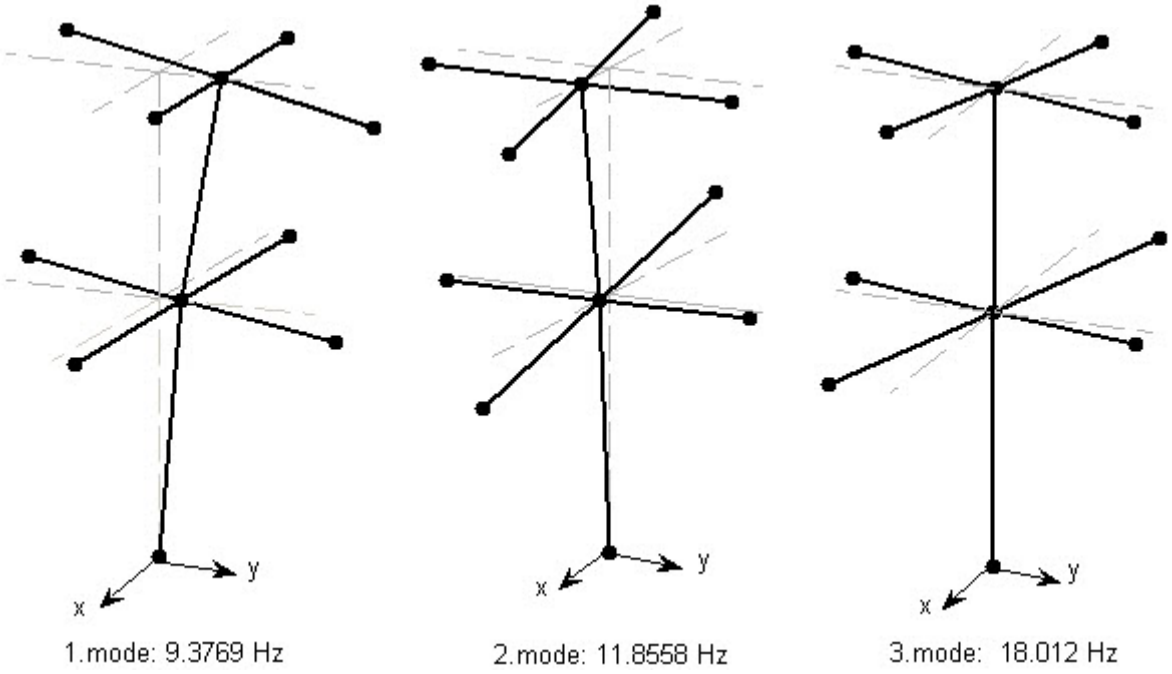

Figure 4.6: Mode shapes of the demo structure

4.3.2 Base excitation simulation

The dynamical acceleration response for base-excited structures is given by eq. **(2.51)**:

$$\{\ddot{v}\} = \sum_{j=1}^{p} \frac{\omega^2 \{Y\}_j \{Y\}_j{}^T ([M][G]\{\ddot{u}_0\})}{k_j - \omega^2 m_j + i\omega c_j}$$

It permits considering the analysis of a situation where the system is simultaneously excited in frequency domain by pure base excitation $\{\ddot{u}_0(\omega)\}$ [4]. So the base acceleration vector $\{\ddot{u}_0\}_{6,1}$ contains maximum acceleration amplitudes. It has to be multiplied with the product of the reduced lumped mass matrix $[M]_{30,30}$ and transformation matrix $[G]_{30,6}$ that is given in Table B.3.

Table 4.1: List of sensors and channels

sensor	x- channel	y-channel	z-channel
A	1	2	3
B	4	5	6
C	7	8	9
D	10	11	12
E	13	14	15
F	16	17	18
G	19	20	21
H	22	23	24
I	25	26	27
J	28	29	30

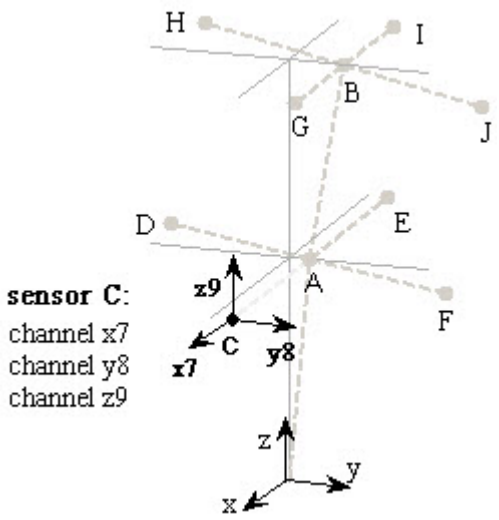

Table 4.1 shows the list of sensors *A*-*J* that virtually "measure" the responses in x-, y- and z-directions. To introduce the response analysis the sensor C is chosen. The "measured" frequency band was limited at 25 Hz. At first a base excitation in only x-direction $\{\ddot{u}_0\} = [1\ 0\ 0\ 0\ 0\ 0]^T$ was applied to demo structure. Figure 4.7 shows the imaginary parts of "measurements" of corresponding channels.

Obviously only the second mode is excited where the first and the third modes are not excited. In accordance with Figure 4.6 where the second mode shape is plotted the sensors "measure" the response amplitudes only in x- and z-direction.

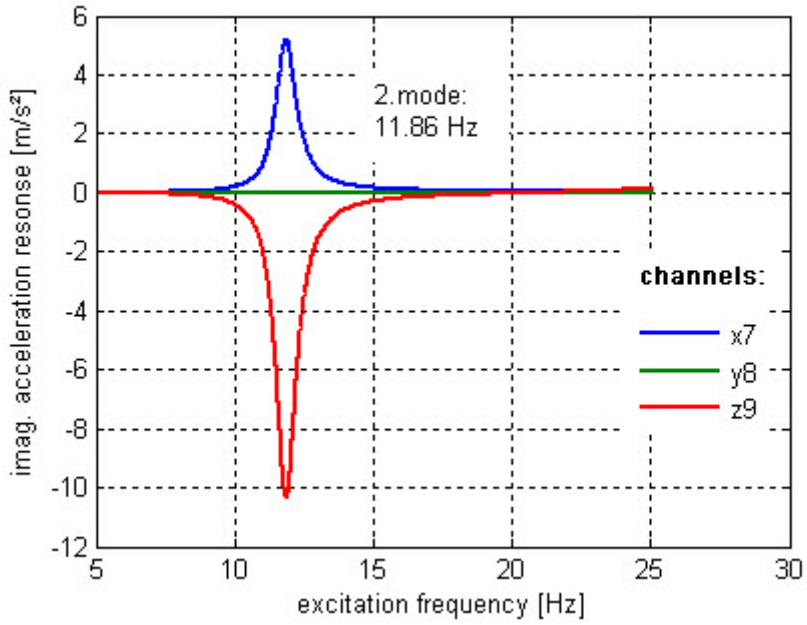

Figure 4.7: Excitation in x-direction

To introduce the cross-talk effect that results in unsolicited motion it is necessary to add the rotational parts to the base excitation vector $\{\ddot{u}_0\}$. Figure 4.8 shows the ancillary effect of an unsolicited rotation about x-axis of the virtual shaker $\{\ddot{u}_0\} = [1\ 0\ 0\ 0.5\ 0\ 0]^T$. According to equations **(2.31)** and **(2.37)** the rotational acceleration part $\ddot{\varphi}_{bx} = 0.5$ has to be multiplied with y- and z-position components of all sensors. The rotational part leads to an additional excitation of the 1.mode that is "measured" by y-channel.

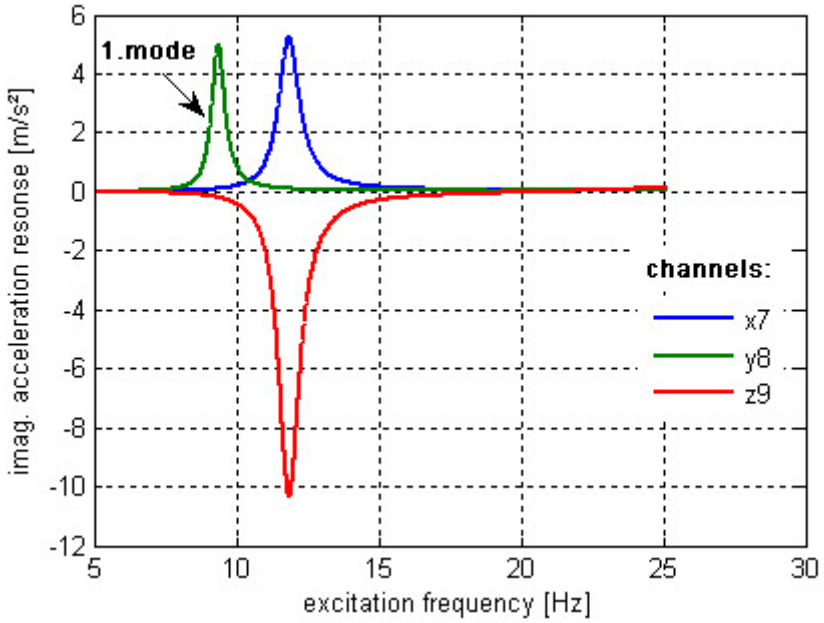

Figure 4.8: Excitation in x- and rotational part about x-axis

Comparison with pure base excitation in y-direction only $\{\ddot{u}_0\} = [0\ 1\ 0\ 0\ 0\ 0]^T$ shows in Figure 4.9 that y-channels "measure" the response amplitudes in y-direction due to the first mode where the central mast oscillates about the x-axis as shown in Figure 4.6.

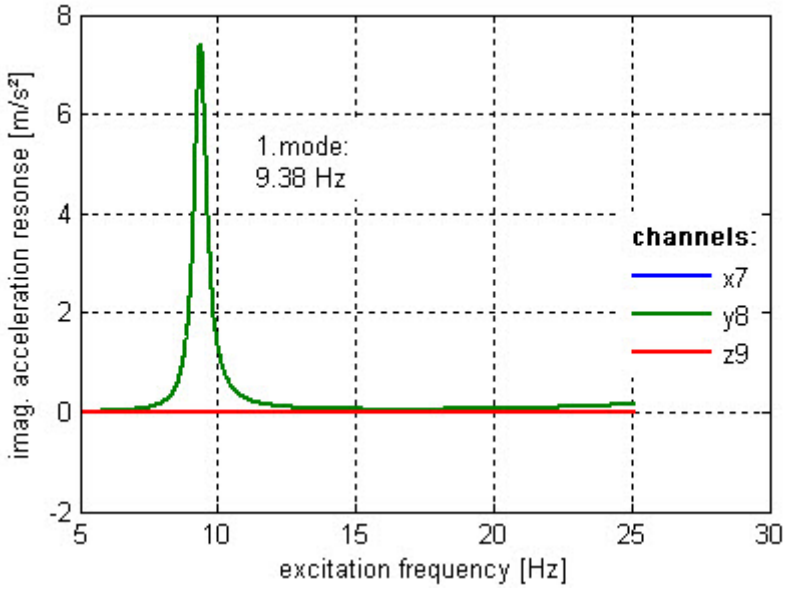

Figure 4.9: Excitation in y-direction

To analyze the unsolicited motion the rotational excitation part $\ddot{\varphi}_{by} = 0.5$ was added to the base excitation vector $\{\ddot{u}_0\} = [0\ 1\ 0\ 0\ 0.5\ 0]^T$. As shown in Figure 4.10 the second mode by side of the first mode is excited.

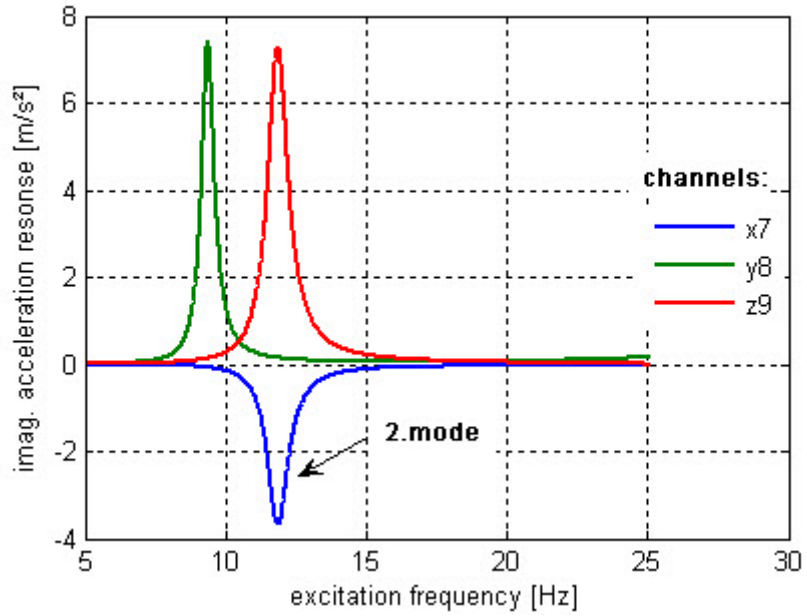

Figure 4.10: Excitation in y-direction with rotational part about y-axis

Figure 4.11 presents the responses where the base excitation in y-direction becomes two rotational acceleration parts $\ddot{\varphi}_{by} = 0.5$ and $\ddot{\varphi}_{bz} = 0.5$. Overall three modes are excited. The third mode is "measured" by y-channel and represents the vibration as shown in Figure 4.6 where the rectangular blades oscillate about z-axis.

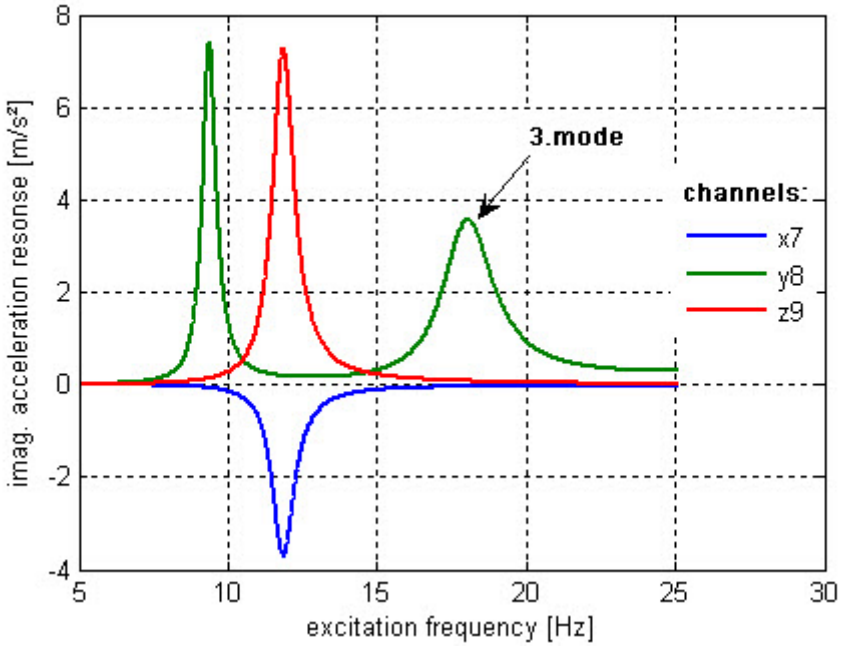

Figure 4.11: Excitation in y-direction with two rotations part

5 Applications

The presented theory in chapter 3 is implemented into a MATLAB-function *identification.m* which includes the post-processing of the vibration test data. The identification procedures are shown in Figure 5.1. The input data are the time-independent geometry, measured frequency excitation and relative response matrices. In the first instance the number of effective modes r that is equal to the rank of the identified condensed stiffness and damping matrices is estimated. After solving of the condensed eigenvalue problem (equations **(3.44)** and **(3.48)**) and backtransformation to the measured physical coordinates (eq. **(3.46)**) the eigenvalues will be identified and the mode shapes can be plotted.

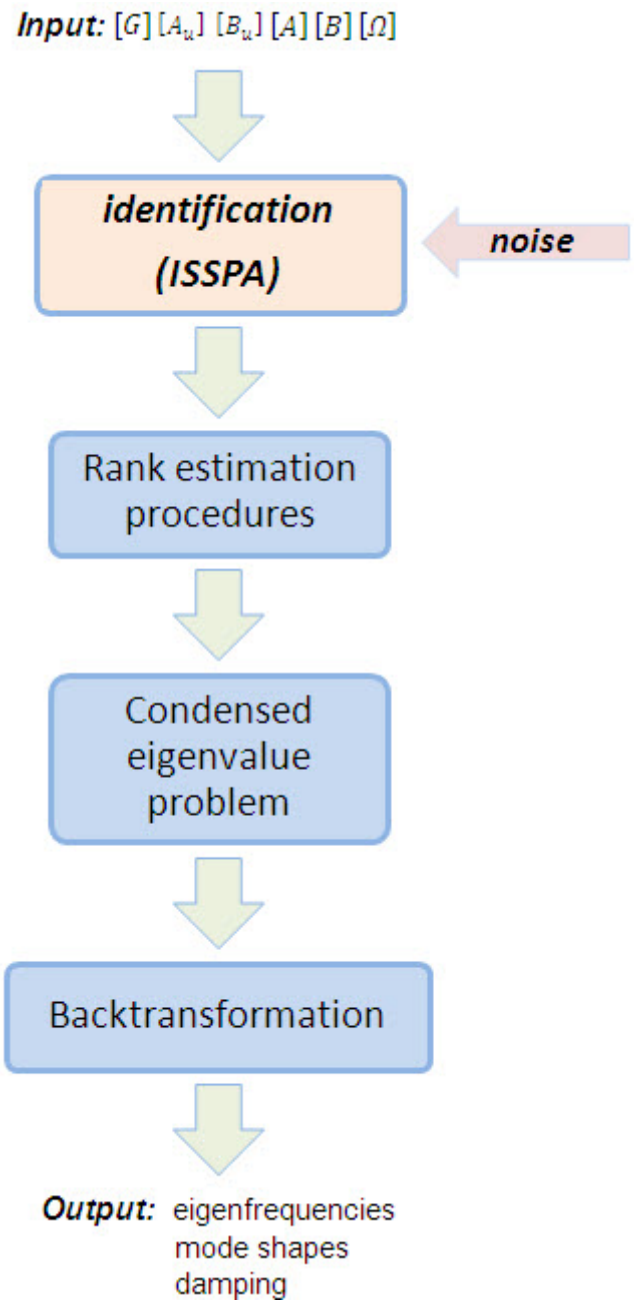

Figure 5.1: Input and output data of *identification.m*

At first demo structure presented in aforementioned chapter was used to test the sensitivity and accuracy of the identification procedure (ISSPA). Subsequently the MATLAB-function *identification.m* was applied to the vibration test data of the original aircraft section in order to demonstrate system identification.

5.1 Application of ISSPA on Demo Structure

The 30-DOF demo structure presented in the chapter 4 was used to test the sensitivity and accuracy of the identification procedure (ISSPA). The reason for the use of simulated test data is the possibility of investigating all influences on the accuracy of the identification method separately [14]. The following influences were investigated

- incomplete frequency range input
- cross-talk
- number of effective degrees of freedom
- measurement errors, by adding random data to the analytical model response
- weakly excited modes

5.1.1 Incomplete frequency range and influence of the cross-talk effect

To render the identification even more difficult the "measured" frequency band was truncated at $24\,Hz$ to establish the incompleteness condition that the MDOF number $p = 30$ is larger than the effective mode number r. The base excitation in the y-direction includes unsolicited rotational parts about y-axis and z-axis $\{\ddot{u}_0\} = [0\ 1\ 0\ 0\ 0.5\ 0.5]^T$. Figure 5.2 shows the "measured" imaginary parts of acceleration responses. The experimental test environment was performed by adding of the random data of 10% to the analytical response data.

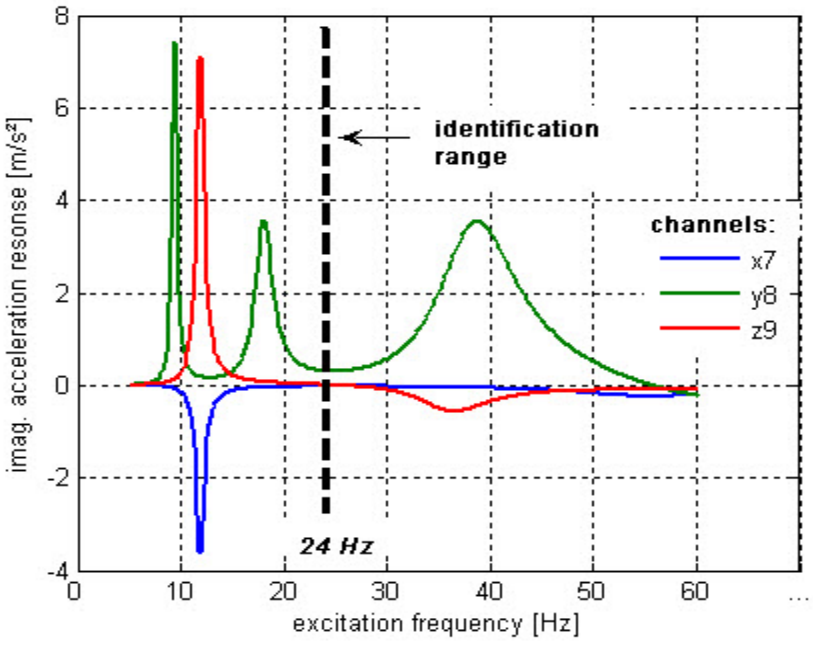

Figure 5.2: Digitized measured frequency response curves

The ratios of consecutive singular values of the imaginary part measurement matrix B ($m = 1011$ frequency points, $p = 30$ MDOF) plotted in Figure 5.3 clearly indicate that at least $r = 3$ effective modes are active in that frequency range.

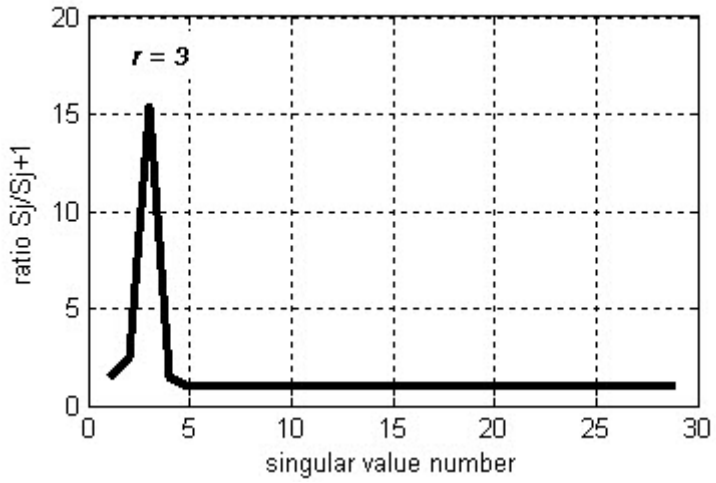

Figure 5.3: Ratios of consecutive singular values

To prove the rms – deviations at the substitute measurement matrix $[\tilde{B}]$ according to eq. **(3.35)** have been calculated for different estimates of r. The plot in Figure 5.4 indicates some changes of slope of curve. The steepest change could be at $r = 4$.

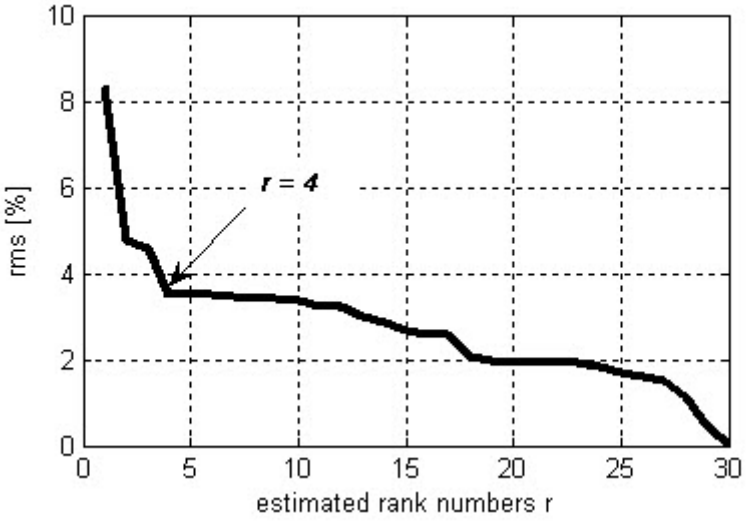

Figure 5.4: rms-deviation of substitute measurement matrix

So a major problem is the determination of the number of the effective degrees of freedom which is equal to the rank of the response matrices. Depending on the individual application it is necessary to run the ISSPA-identification with two or more different numbers of effective degrees of freedom. The best number is then decided on by comparing the measured response data with the recalculated response data using the identified parameters [17].

Figure 5.5 shows the comparison of the recalculated responses as given in eq. **(3.67)** and "measured" responses at sensor C. The responses for $r = 4$ are recalculated with high accuracy whereas the responses for $r = 3$ drift from the "measured" responses.

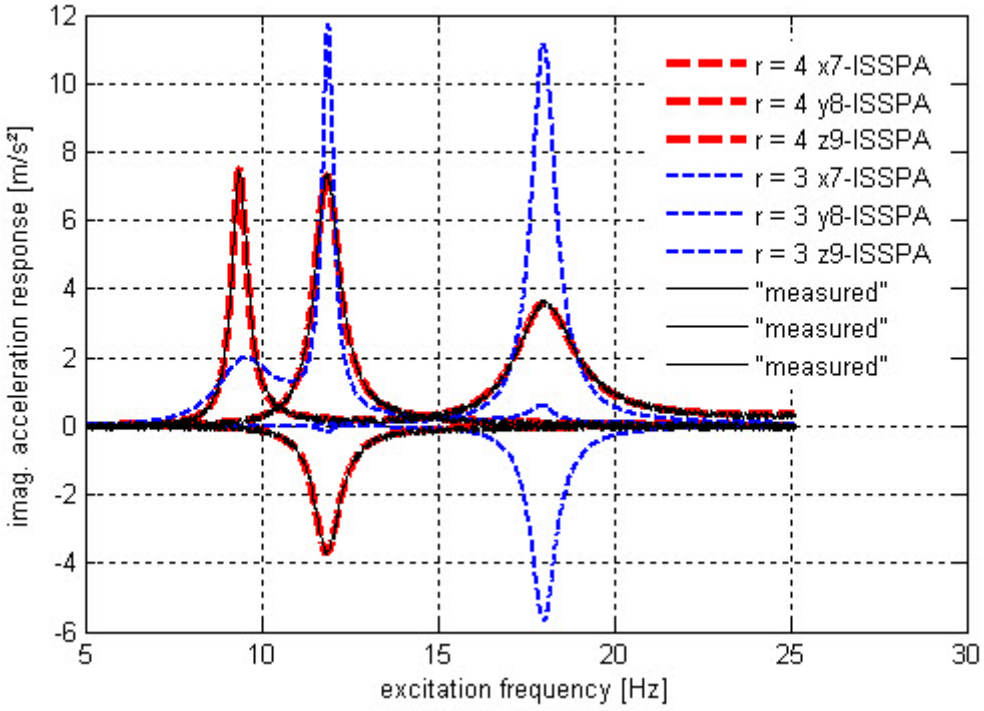

Figure 5.5: Exact and identified responses at channel y8

The identified and analytical mode shapes are correlated by the Modal Assurance Criterion (MAC). The MAC measures the scatter of points between the identified mode shape $\{Y\}$ and the predicted mode shape $\{\psi\}$ [21]:

$$MAC = \frac{[\{Y\}^T\{\psi\}]^2}{[\{Y\}^T\{Y\}][\{\psi\}^T\{\psi\}]} \tag{5.1}$$

Equation **(3.57)** implemented into *identification.m* yield four eigenfrequencies. The following ratios of exact (Table B.2) to identified eigenfrequencies were extracted by comparing of MAC values [7]:

$$\frac{f_{ex}}{f_{id}} = [1.000\ 1.000\ 1.000]$$

Equation **(3.58)** also implemented into *identification.m* yields three corresponding damping values. The ratios of exact (Table B.2) to identified damping values give:

$$\frac{\zeta_{ex}}{\zeta_{id}} = [1.000\ 1.000\ 1.000]$$

Table 4.1summarizes the comparison between exact and identified parameters.

Table 5.1: Identified parameters

mode	**EXACT**		**ISSPA**		
r	f_r $[Hz]$	ζ_r $[-]$	f_r $[Hz]$	ζ_r $[-]$	MAC [%]
1	9.377	0.029	9.378	0.029	100
2	11.856	0.037	11.860	0.037	100
3	18.012	0.057	18.010	0.056	100

The results indicate that the ISSPA-method identifies modal parameters within incomplete frequency range with high accuracy even if the base excitation vector includes rotational parts.

5.1.2 Influence of number of effective degrees of freedom

In a next step the question was investigated how increasing the matrix rank beyond $r = 4$ would influence the identified parameters. The results presented in Table 5.2 for the eigenfrequencies and response compliance indicate that

- increasing the rank estimate beyond $r = 3$ yields pure computational modes
- the eigenfrequencies values of the 3 effective modes can be found and remain stable whereas random deviations of 89.16% were identified between the recalculated and exact responses.
- The best response compliance is at estimated rank $r = 4$

Table 5.2: Identified eigenfrequencies and MAC with respect to different rank estimates r

Rank	**Eigenfrequencies** $[Hz]$			**Damping [-]**			**Response compliance all Sensors**	**Number of noise modes**
r	f_1	f_2	f_3	ζ_1	ζ_2	ζ_3		
	(values in parentheses: deviation to exact solution)							
3	9.476 (−0.099)	11.904 (−0.048)	18.008 (+0.004)	0.021 (+0.09)	0.036 (+0.002)	0.058 (−0.001)	3.949 (−96.051)	-
4	9.381 (−0.004)	11.859 (−0.003)	18.009 (+0.003)	0.029 (±0.000)	0.037 (±0.000)	0.056 (±0.000)	93.111 (+6.889)	1
5	9.379 (−0.002)	11.858 (+0.002)	18.011 (−0.001)	0.029 (±0.000)	0.037 (±0.000)	0.056 (±0.000)	87.729 (+12.270)	2
6	9.380 (−0.003)	11.856 (−0.003)	18.010 (0.002)	0.029 (±0.000)	0.037 (±0.000)	0.056 (±0.000)	92.966 (+7.034)	3
7	9.379 (−0.002)	11.860 (−0.003)	18.005 (0.006)	0.029 (±0.000)	0.037 (±0.000)	0.056 (±0.000)	91.611 (+8.389)	4

5.1.3 Measurement errors, by adding random data to the analytical response

The vibration test data always include noise. In a next step the question was investigated how the different levels of noise influence the identified parameters for estimated rank $r = 4$. The noise was applied by adding uniformly distributed random numbers to the analytical response. Table 5.3 shows the results obtained by the ISSPA for various noise levels.

Table 5.3: Influence of noise

Noise	Eigenfrequencies $[Hz]$			Damping ζ_r [-]			MAC [%] mode shapes		
	f_1	f_2	f_3	ζ_1	ζ_2	ζ_3	*1*	*2*	*3*
	(values in parentheses: relative deviation to exact solution in %)								
zero	9.37 (−0.03)	11.85 (−0.02)	18.02 (+0.03)	0.029 (±0.000)	0.037 (±0.000)	0.057 (±0.000)	100	100	100
10%	9.38 (+0.01)	11.86 (+0.01)	18.01 (−0.01)	0.029 (±0.000)	0.037 (±0.000)	0.057 (±0.000)	100	99.98	99.93
20%	9.39 (+0.21)	11.86 (+0.01)	18.01 (−0.01)	0.027 (−0.068)	0.037 (±0.000)	0.056 (−0.034)	99.99	99.99	99.95
30%	9.40 (+0.29)	11.88 (+0.22)	18.00 (−0.05)	0.026 (−11.389)	0.036 (−3.410)	0.056 (−0.034)	99.99	99.97	99.96
40%	9.43 (+0.52)	11.88 (+0.22)	17.95 (−0.32)	0.025 (−15.96)	0.036 (−3.410)	0.055 (−2.707)	99.99	99.89	99.93

The modal parameters remain stable up to a noise level of 20%. So the ISSPA method can be applied under experimental test environment to identify modal parameters.

5.1.4 Weakly excited modes

In order to study the ability of the identification procedure to extract weakly excited modes caused by increased damping or cross-talk effects the same base excitation vector becomes weakly rotational part about z-axis:$\{\ddot{u}_0\} = [0\ 1\ 0\ 0\ 0.5\ 0.03]^T$. Figure 5.6 shows the very small response peak that is "measured" by channel $y8$. To perform the experimental test environment the random data of 10% were added to analytical response data.

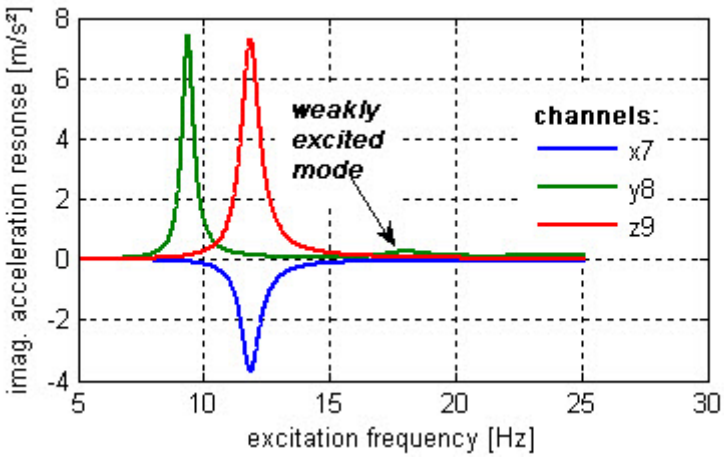

Figure 5.6: Weakly excited mode

The ratios of consecutive singular values as shown in Figure 5.7 clearly indicate that at least $r = 2$ effective modes are “active” in that frequency range. To prove this the rms-deviations at the substitute measurement matrix have been calculated for different estimates of r.

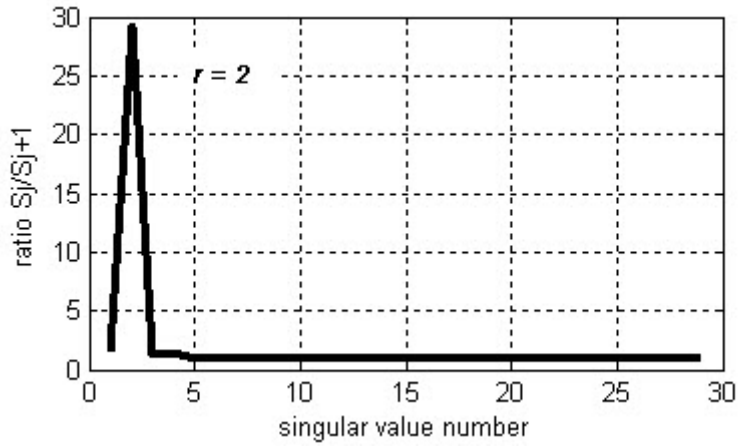

Figure 5.7: The ratios of consecutive singular values in the case of weakly excited mode

To prove the rms – deviations at the substitute measurement matrix $[\tilde{B}]$ according to eq. **(3.35)** have been calculated for different estimates of r. The plot in Figure 5.8 indicates steepest change at $r = 4$.

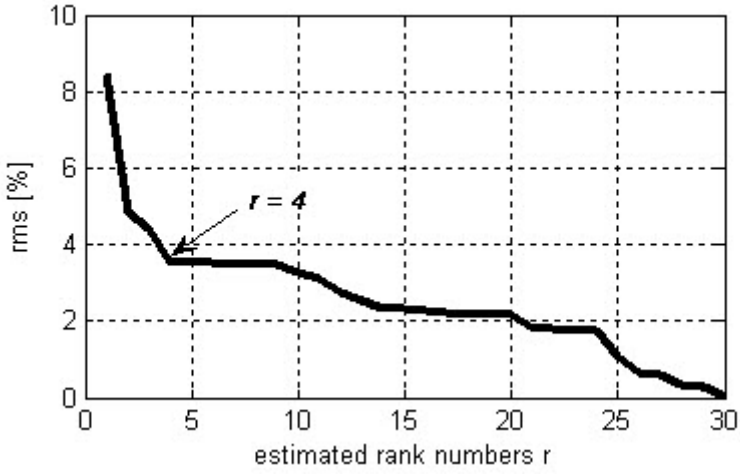

Figure 5.8: rms- deviation in the case of weakly excited mode

Figure 5.9 shows the comparison of the recalculated responses as given in eq. **(3.67)** and “measured” responses at sensor C. The responses for $r = 4$ are recalculated with high accuracy whereas the responses for $r = 2$ drift from the “measured” responses.

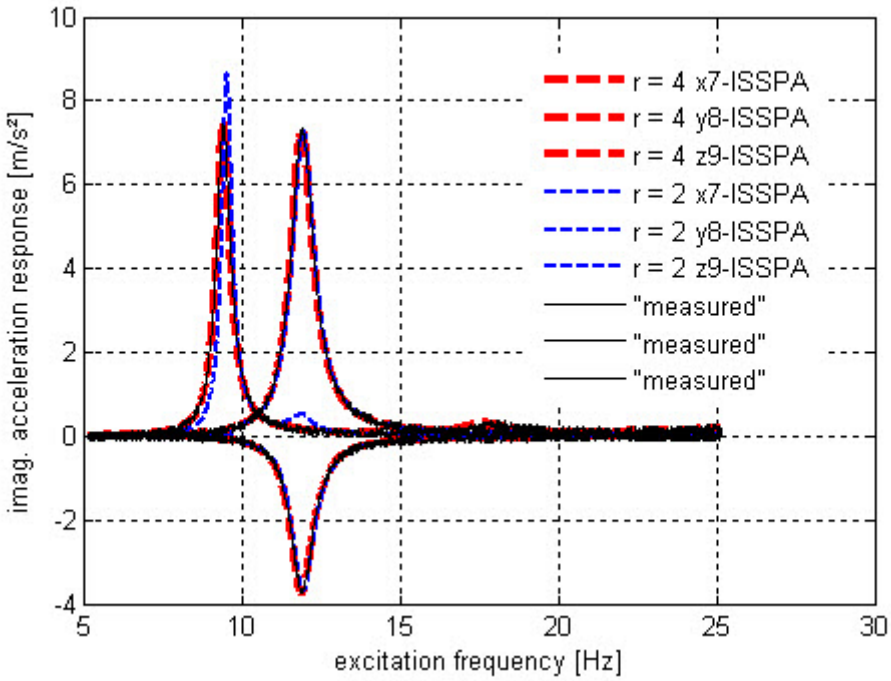

Figure 5.9: Recalculating responses in the case of weakly excited mode

The next investigated question was whether changing the matrix rank beyond $r = 4$ would either allow the identification of the "hidden" mode or would only produce additional modes. The results presented in

Table 5.4 for the eigenfrequencies and damping values indicate that

- the weakly excited mode cannot be extracted
- increasing rank beyond $r = 2$ produces noise modes
- only two eigenmodes can be extracted from noise modes
- the best response compliance of all responses (93.10 %) is at estimated rank $r = 4$

Table 5.4: Identified parameters in the case of weakly excited mode

Rank	**Eigenfrequencies** $[Hz]$			**Damping** ζ_r [-]			**Response compliance [%]**
	f_1	f_2	f_3	ζ_1	ζ_2	ζ_3	
	(values in parentheses: deviation to exact solution)						
2	9.509 (−0.132)	11.916 (−0.060)	-	0.021 (+0.008)	0.037 (+0.001)	-	85.391 (+14.609)
4	9.382 (−0.005)	11.858 (−0.002)	*noise*	0.029 (±0.000)	0.037 (±0.000)	*noise*	93.108 (+6.892)
7	9.379 (−0.002)	11.859 (−0.003)	*noise*	0.029 (±0.000)	0.037 (±0.000)	*noise*	85.391 (+14.609)

5.2 Application of ISSPA to Vibration Test Data from the Aircraft Section

In order to demonstrate the parameter identification method, the MATLAB-function *identification.m* was applied to the vibration test data of the original aircraft section. The vibration test was accomplished on the electrohydraulic exciter.

Figure 5.10 shows the principle test set-up. The test fixture is an adapter system that was connected to the test specimen and the shaker table. It has its first eigenfrequency above the investigated frequency range. Four tri-axial accelerometers were placed on the shaker table to measure input excitation acceleration. The sensors on the section measure the absolute acceleration responses.

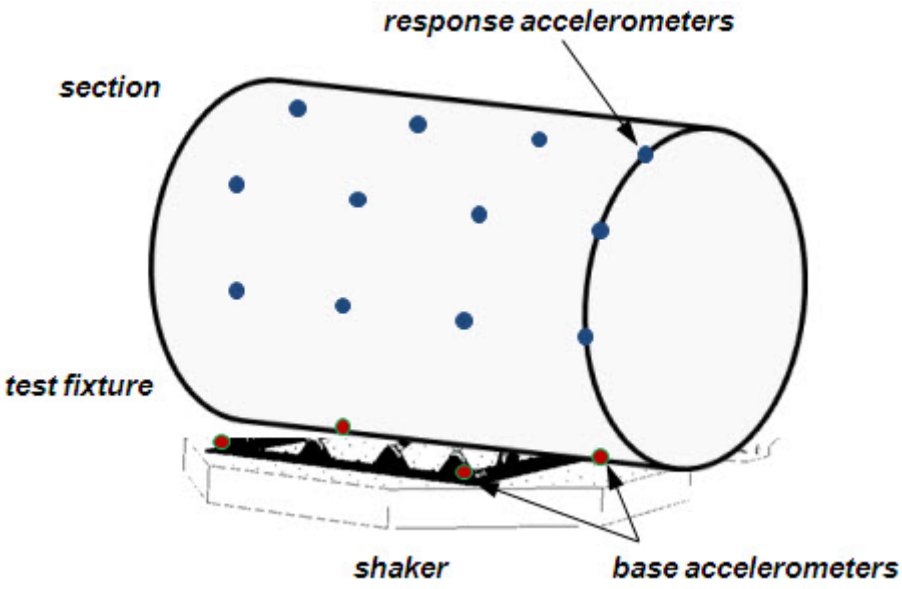

Figure 5.10: Aircraft section

The real and imaginary acceleration response data were available from a sinusoidal sweep base excitation at 101 measurement degrees of freedom digitised at 1188 frequency points. Only $p = 77$ degrees of freedom were retained for the ISSPA identification. The frequency range of investigation is normalized to unity. The real part data are assembled in the matrix $[A]$, the imaginary part data in the trix$[B]$. Each column of these matrices represents the frequency response curve of one measuring degrees of freedom that are also normalized to unity.

5.2.1 Identification in the case of base excitation in y-direction

In a first step the identification-method was applied to the vibration test data in the case of base excitation in the y-direction. Figure 5.11 shows the measured unsolicited motions of the shaker because of crass-talk effects.

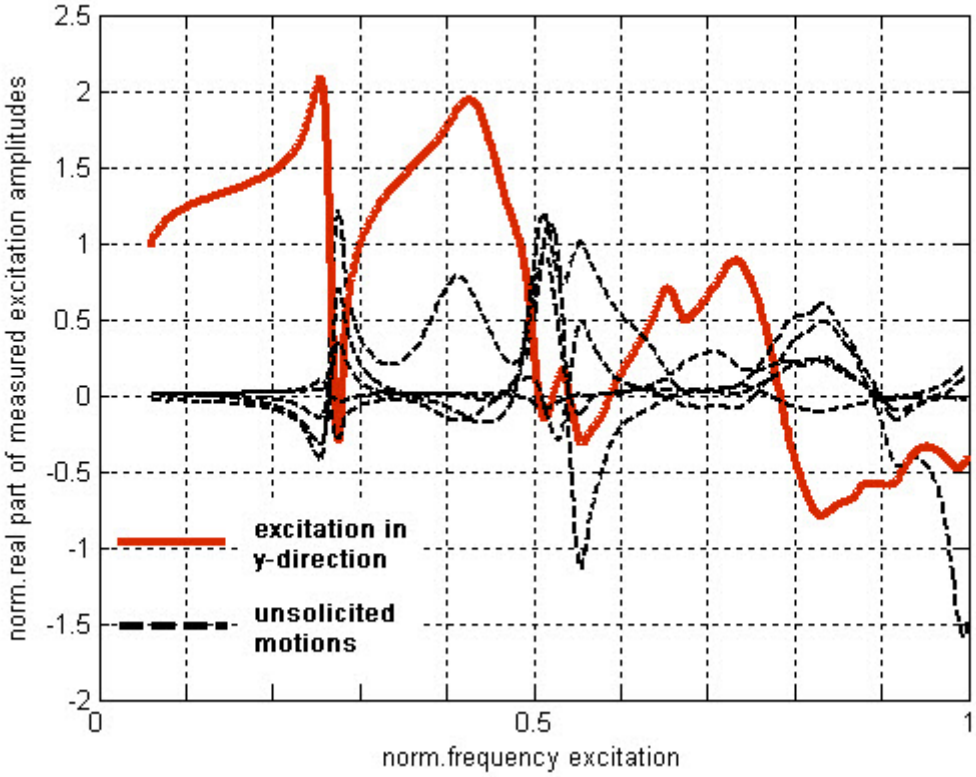

Figure 5.11: Unsolicited motions of the shaker

Figure 5.12 shows the imaginary part of normalized acceleration response at channel no. 55 that measures the response in y-direction.

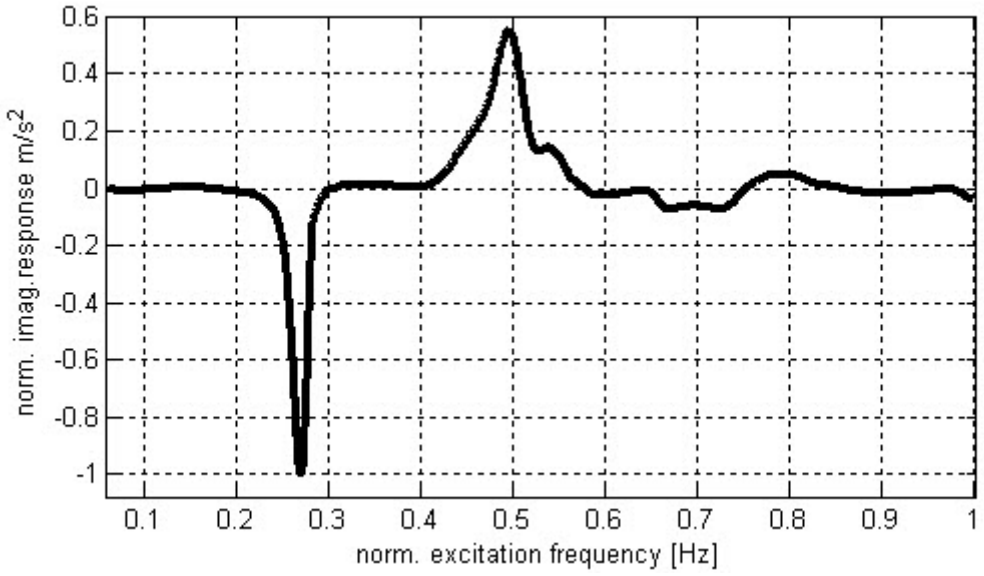

Figure 5.12: Normalized imaginary acceleration response at channel 55

Due to unknown measurement errors sources and non-linearity effects the ratios of consecutive singular values of the measurement matrices plotted in Figure 5.13 show several definite peaks whereas the magnitudes at $r = 3$ and $r = 6$ are most significant.

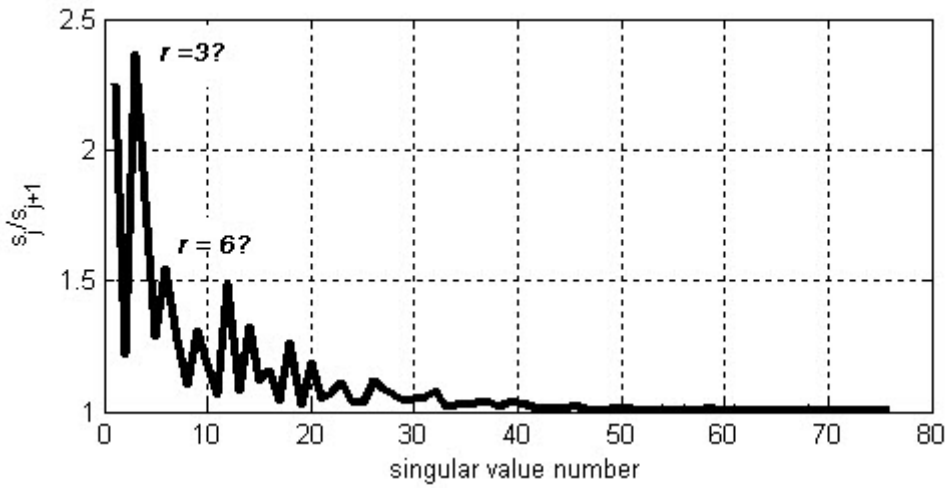

Figure 5.13: Ratios of consecutive singular values

The rms-deviation in Figure 5.14 also indicates several changes of slope of that curve. Whereas the change at $r = 6$ shows to be the steepest.

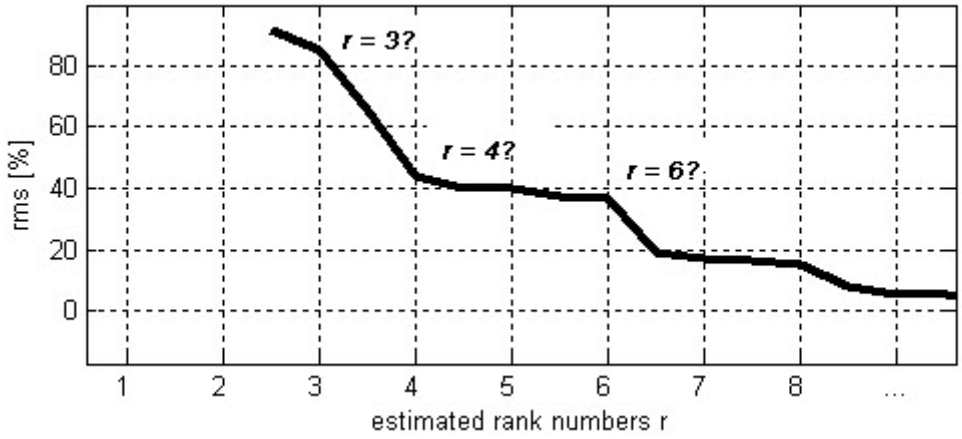

Figure 5.14: rms-deviation of substitute measurement matrix

Table 5.5 shows the summary of the accomplished rank analysis

- Estimate of $r = 3$ gives no noise modes and reasonable eigenfrequency ratios but no clear compliance between the recalculated and measured responses (72.04%).
- Estimate of $r = 6$ gives three noise modes. The response compliance accounts for 81.35%. Three eigenfrequencies could be extracted by comparing of corresponding identified and analytical mode shapes. The extracted eigenfrequency ratios are also plausible.
- Tee best response compliance accounts for 89.52% for estimate rank $r = 5$.
- The clear statement about the damping is impossible because the analytical damping model is not present but all identified damping values are in the plausible range $(0.06\% - 2.87\%)$.

Table 5.5: Rank analysis

rank	*eigenfrequency ratio* $f_r\,[f_{sim}/f_{id}]$			*damping* ζ *[%]*			*resp.compl. [%]*	*noise mode*
	f_{r1}	f_{r2}	f_{r4}	ζ_1	ζ_2	ζ_4		
3	1.04	1.16	1.29	1.39	0.96	0.49	72.036	-
4	1.07	1.16	1.34	0.67	1.05	0.37	0.987	1
5	1.07	1.17	1.31	0.06	1.13	2.87	89.521	2
6	1.08	1.16	1.34	0.33	1.03	1.91	81.346	3

However, from comparing the recalculated and the measured responses as shown in Figure 5.15, the best agreement was obtained using the rank estimate $r = 5$.

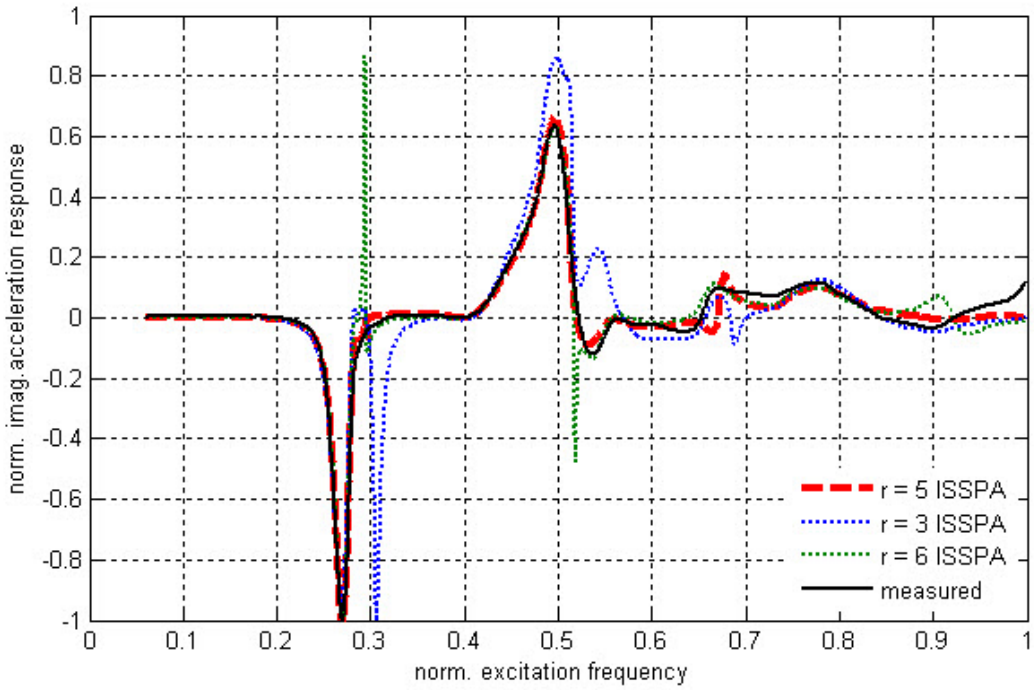

Figure 5.15: Comparison of recalculating responses

It should be denoted out that ISSPA, in contrast to other exciting modal identification methods, is not a response curve fitting method, i.e. good agreement between the measured and recalculated response must also be a measure of the accuracy of the physical system matrix $[K^*]$, which is not identified in standard curve fitting procedures [14]. Figure 5.16 shows the real and imaginary part responses of an arbitrary DOF $no.55$ that were recalculated with high accuracy.

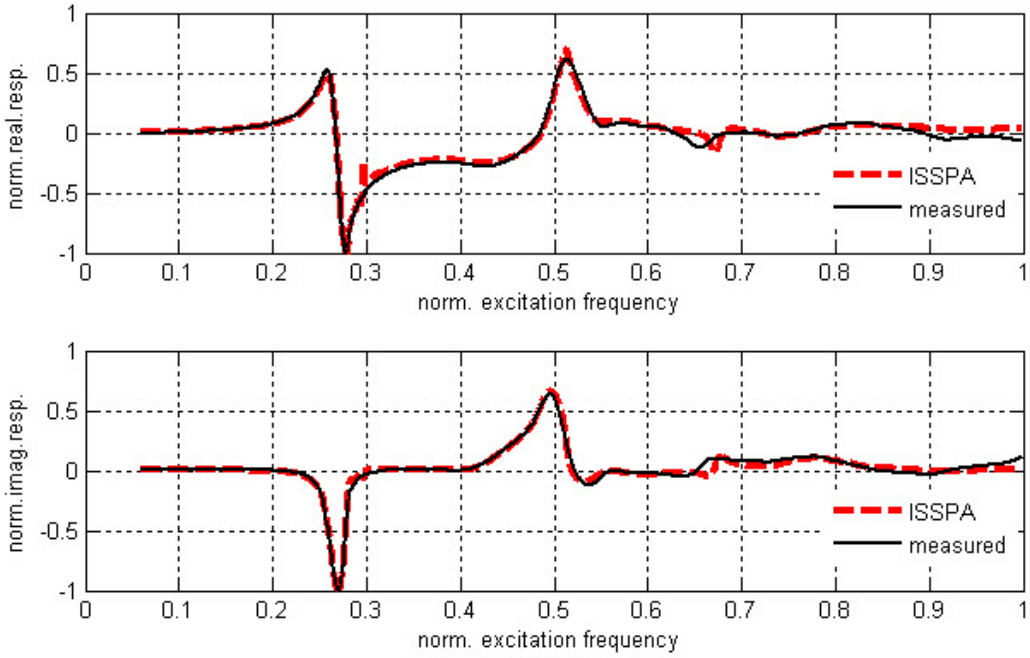

Figure 5.16: DOF no.55: real and imaginary part responses

Table 5.6 summarizes the identified modal parameters for the rank estimate $r = 5$ and Figure 5.17 represents the corresponding mode shapes that were identified.

Table 5.6: Identified modal parameters for rank r = 5 in the case of y-excitation

Mode no.	*Eigenfrequency ratio* f_r $[f_{sim}/f_{id}]$	*Damping* ζ *[%]*	*MAC [%]*
1	1.07	0.06	97.71
2	1.16	1.13	82.49
4	1.31	2.87	82.76

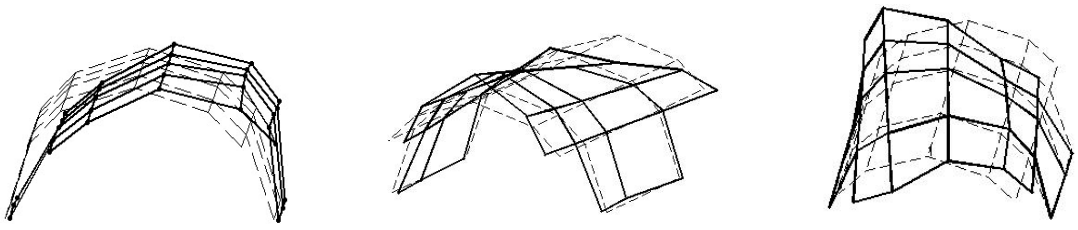

Figure 5.17: Identified mode shapes for estimate rank r = 5 in the case of y-excitation

5.2.2 Identification in the case of base excitation in z-direction

In the next step the identification in the case of the base excitation in z-direction using the selected frequency band is accomplished. The Figure 5.18 shows the selected frequency range around the distinct peak in which the identification will be performed. Cutting out of this frequency band should minimize noise effects.

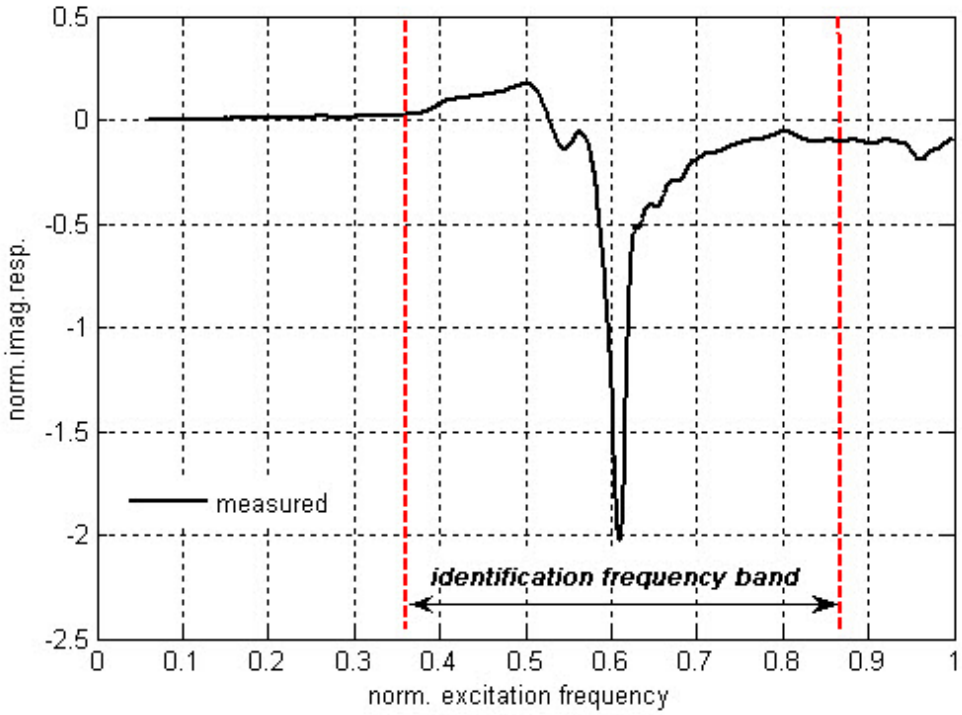

Figure 5.18: Identification frequency band

Comparison of the recalculated and measured responses as shown in Figure 5.19 indicates the best decision is to use the rank $r = 5$.

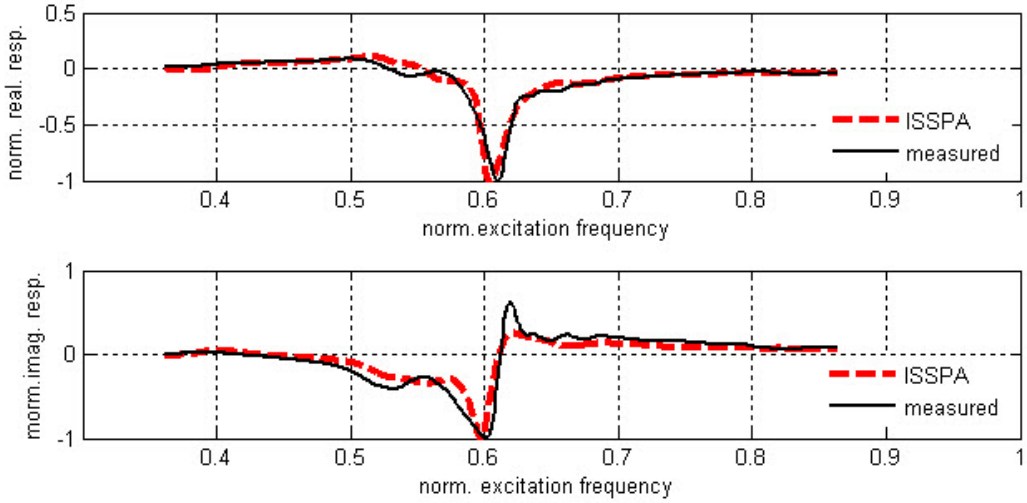

Figure 5.19: DOF no.37: real and imaginary part responses

As shown in Table 5.7 three eigenvalues and eigenmodes are identified from the selected frequency band.

Table 5.7: Identified modal parameters for estimate rank r = 5 in the case of z-excitation

Mode no.	*Eigenfrequency ratio* f_r $[f_{sim}/f_{id}]$	*Damping* ζ *[%]*	*MAC [%]*
2	1.11	0.32	81.16
3	1.14	1.32	95.35
4	1.29	1.22	84.34

The identified mode shapes are presented in Figure 2.1

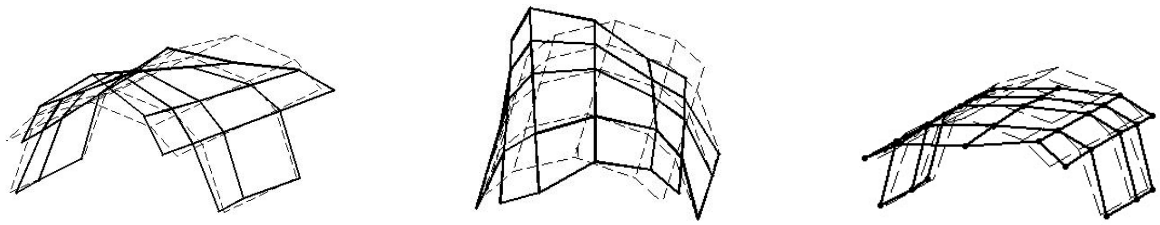

Figure 5.20: Identified mode shapes for estimate rank r = 5 in the case of z-excitation

5.2.3 Results overview

The programmed MATLAB-function *identification-m* is effective applied to the vibration test data of the original aircraft section. In the first step the test data from the lateral excitation (y-direction) are used. First, second and fourth predicted eigenfrequencies are identified for estimate rank $r = 5$. The identified mass-modified system matrices enable to recalculate the responses with high accuracy. In the next step the test data from the z-excitation are used. The identification frequency band is selected to minimize the noise errors. Second, third and fourth predicted eigenfrequencies are identified for estimate rank $r = 5$.

6 Conclusion and Outlook

The objective of this thesis was the application of the identification method to real vibration data in order to identify modal parameters like eigenfrequencies, mode shapes and damping. The identification method has to consider the interaction between the multi-axis shaker and the test specimen. The identified modal parameters are essential for the following validation of FEM-models and can conclusively improve the design of the investigated structures.

The correct equation of motion for multi-axial base excited MDOF-systems is a requirement for the modal analysis of such structures that are excited by shakers. The thorough derivation of the equation of motion was discovered in [6] and [11]. After the research of the best applicable identification methods, the method called ISSPA (Identification of Structural System Parameters), developed by M.Link, was detected in [13], [14], [15], [16] and [17]. The theory was extracted and implemented with MATLAB: *identification.m*

In order to check the sensitivity and accuracy of the function *identification.m* with respect to conditions that represent many practical test situations a virtual 3D demo structure was required. The demo structure was specially designed with MATLAB-tool *demostructure.m* that constructs system matrices, eliminates redundant DOFs and accomplishes the eigenvalue problem. The material properties of the demo structure were obtained in [1]. An additional programmed MATLAB-function *response_analysis.m* enables the forced response analysis where effects of unsolicited motions of the virtual shaker can be simulated.

Finally the function *identification.m* was successful applied to the measured frequency test data of the original aircraft section. The test data were extracted for the base excitation in y-direction where the unsolicited motions of the shaker in directions of all the rest DOFs were also ascertained. The original measurement matrices were modified such that their rank was equally to the number r of effective modes. Without this modification there would be no rank defect in the original measurement matrices due to measuring errors and unavoidable non-linearities. The difficulty was the investigation of the correct number of effective modes. There are many different procedures to extract the effect of noise modes from the identification equation. From comparing the recalculated and the measured responses best agreement was obtained using the rank $r = 5$. By comparing of MAC values three eigenfrequencies and modes and three computational modes have been identified. These eigenvalues were predicted by analytical model and can be used for its validation.

Furthermore ISSPA yields not only modal data but also physical system matrices that can be used for updating analytical models in order to identify those areas on the structure where modifications of the physical stiffness, mass, and damping parameter have to be applied. Comparison of the finite element and identified dynamic matrices makes it possible to identify deviations of the mathematical model in physical coordinates. It should be denoted that the comparison for the mass modified system is possible only in case of known base reactions forces which have to be measured during the test.

ISSPA is the frequency-domain identification. But it is also reasonable to apply the time-domain identification to the same vibration test data in time-domain to identify the modal parameter that can be compared with the results of the frequency-domain identification ISSPA.

References

[1] Breitbach E.J. – Experimentelle Simulation Dynamischer Lasten an Raumfahrtsystemen mittels modaler Erregerkraftkombinationen, Habilitationsschrift, 1988

[2] Clough R.W, Penzien J. – Dynamics of Structures, 1995

[3] Cook R.D. - Finite Element Modelling for Stress Analysis, 1995

[4] Ewins D.J. – Modal Testing: Theory and Practice

[5] Freymann R. - Strukturdynamik, Ein Anwendungsorientiertes Lehrbuch, 2011

[6] Füllekrug U. – Utilization of multi-axial shaking tables for the modal identification of structures, Phil. Trans. R. Soc. Lond. A September 15, 2001

[7] Füllekrug U., Sinapius J.M. – Strukturdynamische Identifikation bei mehrachsiger Anregung, 1998

[8] Graham S.K. – Fundamentals of Mechanical Vibrations, 2000

[9] Guyan J.R. – Reduction of Stiffness and Mass Matrices, AIAA Journal 3(2), 380, 1965

[10] He J., Fu Z. – Modal Analysis, 2001

[11] Jagmohan L.H. – Dynamic of Structures, 2001

[12] Lanczos C. – The Variational Principles of Mechanics, 1986

[13] Link M. – Baudynamik und Systemidentification, Der Ingenieurbau, B5, 1995

[14] Link M. – Application of a Method for Identifying Incomplete System Matrices Using Vibration Test Data, Zeitschrift für Flugwissenschaten und Weltraumforschung 9, 1985, pp.178-187

[15] Link M. – Theory of a Method for Identifying Incomplete System Matrices from Vibration Test Data, Zeitschrift für Flugwissenschaten und Weltraumforschung 9, 1985, pp.76-82

[16] Link. M. – On the Determination of the Effective Modes from Vibration Test Data, 1988

[17] Link. M., Vollan A. – Identification of Structural System Matrices from Vibration Test Data, Zeitschrift für Flugwissenschaten und Weltraumforschung 2, 1978, pp.165-174

[18] McConnel K.G. – Vibration Testing, Theory and Practice, 1995

[19] Paz M., Leigh W. – Structural Dynamics, Theory and Computation, 2004

[20] Sinapius J.M. - Experimental Dynamic Load Simulation by Means of Modal Force Combination, Aerospace and Technology, 1997, 4, 267-275

[21] Sinapius J.M., Gloth G., Polster M. – Review of Data Reduction Techniques for the Interpretation of Dynamic Qualification with Swept-Sine Excitation

A Electrohydraulic Exciter

Table A.1: Typical technical parameters of electrohydraulic exciter

Feature	Parameters
Size of table platform	$4.0m \times 4.0m$
Table mass	$\sim 22000kg$
Lowest eigenfrequency	$> 100\ Hz$
Number of vertical actuators	4
Number of horizontal actuators	4
Number of hydraulic pumps	5
Power rating	$1000kVA$
Maximum oil flow	$1750\ l/min$
Maximum play load	$15000kg$
Maximum way	$0-2\ Hz: \pm 70\ mm/s$
Maximum velocity	$2-10\ Hz: \pm 0.8\ m/s$
Maximum acceleration: empty table	$\pm 60\ m/s^2\ (vertical);\ \pm 35 m/s^2 (horizontal)$
Maximum acceleration: maximum play load	$\pm 34\ m/s^2\ (vertical);\ \pm 22 m/s^2 (horizontal)$

B Demo Structure Properties

B.1 Material and geometry properties

Table B.1: Material properties of a demo structure

Beam-element	Final weight mi [kg]	Length a [m]	Reference axis u	Bending stiffness EIu 10^5 Nm²	Reference axis v	Bending stiffness EIv 10^5 Nm²	Torsion stiffness GId 10^5 Nm²	Stress stiffness EA 10^8 N
1-2	60	0,8	x	4,16	y	7,04	4,43	5,12
2-3	40	0,7	x	4,16	y	7,04	4,43	5,12
2-4	14	0,8	y	1,28	z	1,92	1,48	1,92
2-5	17	0,5	x	1,28	z	1,92	1,48	1,92
2-6	9	0,8	y	1,28	z	1,92	1,48	1,92
2-7	17	0,5	x	1,28	z	1,92	1,48	1,92
3-8	9	0,5	y	1,28	z	1,92	1,48	1,92
3-9	11	0,5	x	1,28	z	1,92	1,48	1,92
3-10	9	0,5	y	1,28	z	1,92	1,48	1,92
3-11	11	0,5	x	1,28	z	1,92	1,48	1,92

B.2 Eigenvalues

Table B.2: Eigenfrequencies and damping values

Mode Nr.	Eigenfrequency [Hz]	Damping ζ	Mode Nr.	Eigenfrequency [Hz]	Damping ζ
1	9,38	0,0295	16	92,21	0,2897
2	11,86	0,0372	17	108,65	0,3413
3	18,01	0,0566	18	113,24	0,3558
4	36,22	0,1138	19	132,89	0,4175
5	36,79	0,1156	20	135,05	0,4243
6	38,44	0,1208	21	380,30	1,1947
7	39,74	0,1248	22	658,96	2,0702
8	51,50	0,1618	23	756,42	2,3764
9	54,57	0,1714	24	801,21	2,5171
10	60,87	0,1912	25	940,40	2,9542
11	66,19	0,2079	26	948,40	2,9795
12	67,32	0,2115	27	953,35	2,9950
13	83,04	0,2609	28	1039,60	3,2660
14	83,28	0,2616	29	1172,18	3,6825
15	90,85	0,2854	30	1253,16	3,9369

B.3 Transformation matrix

Table B.3: Transformations matrix

1	0	0	0	0.8	0
0	1	0	-0.8	0	0
0	0	1	0	0	0
1	0	0	0	1.5	0
0	1	0	-1.5	0	0
0	0	1	0	0	0
1	0	0	0	0.8	0
0	1	0	-0.8	0	0.8
0	0	1	0	-0.8	0
1	0	0	0	0.8	0.5
0	1	0	-0.8	0	0
0	0	1	-0.5	0	0
1	0	0	0	0.8	0
0	1	0	-0.8	0	-0.8
0	0	1	0	0.8	0
1	0	0	0	0.8	-0.5
0	1	0	-0.8	0	0
0	0	1	0.5	0	0
1	0	0	0	1.5	0
0	1	0	-1.5	0	0.5
0	0	1	0	-0.5	0
1	0	0	0	1.5	0.5
0	1	0	-1.5	0	0
0	0	1	-0.5	0	0
1	0	0	0	1.5	0
0	1	0	-1.5	0	0.5
0	0	1	0	0.5	0
1	0	0	0	1.5	-0.5
0	1	0	-1.5	0	0
0	0	1	0.5	0	0

C MATLAB scripts

C.1 Main design

```
% MAIN DESIGN
% Author: Dimitrij Shulkin, 2012
% ========================================================================
clc; close all; clear all;
[properties] = demo_structure_properties
%=========================================================================
%                       REDUCED STIFFNESS AND MASS MATRICES
%=========================================================================
[K M G]                   =   demostructure(properties);
%=========================================================================
%                         BASE EXCITATION SIMULATION
%=========================================================================
%                          translational  rotational
%                            x   y   z    x   y   z
                       ub = [1   0   0    1   0   0]';
[X wr sr plotnumber]      =   response_analysis(K,M,G,ub,properties)
%=========================================================================
%                                    ISSPA
%=========================================================================
%                                 INTERFACE
% Analytical data of demo structure
[A B Au Bu Omega]         =   interface(X,wr,sr,ub);

%                               IDENTIFICATION
% Choose effective dof:
effdof                    = 2;
[frr drr]                 = identification(A,B,Au,Bu,G,Omega,plotnumber,effdof)
```

C.2 *demostructure.m*

```
function [K M G] = demostructure(properties)
%=========================================================================
% Procedures of the reduction of the system matrices of the demo structure
% INPUT DATA      : material and gemoetry properties of demo structure
% Author          : Dimitrij Shulkin 2012
% =========================================================================
% Parameters of demo structure
m                       =   properties.m;    % mass [kg]
L                       =   properties.L;    % lengths [m]
EA                      =   properties.EA;   % length stiffness [N]
EIx                     =   properties.EIx;  % bending stiffness, reference axis x
EIy                     =   properties.EIy;  % bending stiffness, reference axis y
EIz                     =   properties.EIz;  % bending stiffness, reference axis z
GI                      =   properties.GI;   % torsional stiffness
alfa                    =   properties.alfa; % alfa rotation of beams
beta                    =   properties.beta; % beta rotation of beams
gama                    =   properties.gama; % gama rotation of beams
n                       =   properties.n;    % quantity of beams
dof                     =   properties.dof;  % global degrees of freedom
G                       =   properties.G;
% Incidence table                                       % beam number
inz     =   [1 2 3 4 5 6 37 38 39 7 8 9;...             %   1-2
             37 38 39 7 8 9 40 41 42 10 11 12;...       %   2-3
             37 38 39 7 8 9 43 44 45 13 14 15;...       %   2-4
             37 38 39 7 8 9 46 47 48 16 17 18;...       %   2-5
             37 38 39 7 8 9 49 50 51 19 20 21;...       %   2-6
             37 38 39 7 8 9 52 53 54 22 23 24;...       %   2-7
             40 41 42 10 11 12 55 56 57 25 26 27;...    %   3-8
             40 41 42 10 11 12 58 59 60 28 29 30;...    %   3-9
             40 41 42 10 11 12 61 62 63 31 32 33;...    %   3-10
             40 41 42 10 11 12 64 65 66 34 35 36];      %   3-11
% Initialisation
Kglob   =   zeros(dof,dof);
% Assemblage of global stiffness matrix
for i   =   1:n
    Kglob(inz(i,:),inz(i,:)) = Kglob(inz(i,:),inz(i,:)) + ...
    elementstiff-
ness(EA(i),EIx(i),EIy(i),EIz(i),GI(i),L(i),alfa(i),beta(i),gama(i),i);
end;
% Elemination of fixed dof (1 2 3 4 5 6)
Kred    =   Kglob(7:66,7:66);

%=========================================================================
%                       STATIC CONDENSATION METHOD
%=========================================================================
% Paz M., Leigh W. – Structural Dynamics, Theory and Computation, 2004
% secondary rotational degrees of freedom to be reduced
us      =   1:30;
% primarary translational degrees of freedom
um      =   31:60;
Ks      =   Kred(us,us);
Kp      =   Kred(us,um);
% transformation matrix
T       =   -inv(Ks)*Kp;
T       =   [T;eye(30)];
% reduced sitffness matrix
K       =   T'*Kred*T;
%=========================================================================
%                               LUMPED MASS
%=========================================================================
% Paz M., Leigh W. – Structural Dynamics, Theory and Computation, 2004
M       =   diag([m(2) m(2) m(2) m(3) m(3) m(3) m(4) m(4) m(4) m(5) m(5) m(5)...
                  m(6) m(6) m(6) m(7) m(7) m(7) m(8) m(8) m(8) m(9) m(9) m(9)...
                  m(10) m(10) m(10) m(11) m(11) m(11)])
```

C.2.1 Input data for *demostructure.m*

```
function [properties] = demo_structure_properties
%=========================================================================
% OUTPUT DATA:  material and geometry properties of the 3D demo structure
% Taken from:   Breitbach E.J. – Experimentelle Simulation
%               Dynamischer Lasten an
%               Raumfahrtsystemen mittels modaler Erregerkraftkombinationen,
%               Habilitationsschrift, 1988
% Author:       Dimitrij Shulkin, 2012
%=========================================================================
% mass [kg]
properties.m    =   [0 60 40 14 17 14 17 9 11 9 11];
% lengths [m]
properties.L    =   [0.8 0.7 0.8 0.5 0.8 0.5 0.5 0.5 0.5 0.5];
% length stiffness [N]
properties.EA   =   10^8*[5.12 5.12 1.92 1.92 1.92 1.92 1.92 1.92 1.92 1.92];
% bending stiffness, reference axis x
properties.EIx  =   10^5*[4.16 4.16 0 1.28 0 1.28 0 1.28 0 1.28];
% bending stiffness, reference axis y
properties.EIy  =   10^5*[7.04 7.04 1.28 0 1.28 01.28 01.28 0 1.28 0];
% bending stiffness, reference axis z
properties.EIz  =   10^5*[0 0 1.92 1.92 1.92 1.92 1.92 1.92 1.92 1.92];
% torsional stiffness
properties.GI   =   10^5*[4.43 4.43 1.48 1.48 1.48 1.48 1.48 1.48 1.48 1.48];
% rotation of beams
properties.alfa =   [0 0 0 0 0 0 0 0 0 0];
properties.beta =   [pi/2 pi/2 0 0 0 0 0 0 0 0];
properties.gama =   [0 0 0 pi/2 pi -pi/2 0 pi/2 pi -pi/2];
% quantity of beams
properties.n    =   10;
% global degrees of freedom
properties.dof  =   66;
% Geometric transformation matrx
properties.G = [1 0 0 0 -0.8  0;   0 1 0 0.8 0  0;     0 0 1  0   0    0;...
                1 0 0 0 -1.5  0;   0 1 0 1.5 0  0;     0 0 1  0   0    0;...
                1 0 0 0 -0.8  0;   0 1 0 0.8 0  0.8;   0 0 1  0  -0.8  0;...
                1 0 0 0 -0.8 -0.5; 0 1 0 0.8 0  0;     0 0 1  0.5 0    0;...
                1 0 0 0 -0.8  0;   0 1 0 0.8 0 -0.8;   0 0 1  0   0.8  0;...
                1 0 0 0 -0.8  0.5; 0 1 0 0.8 0  0;     0 0 1 -0.5 0    0;...
                1 0 0 0 -1.5  0;   0 1 0 1.5 0  0.5;   0 0 1  0  -0.5  0;...
                1 0 0 0 -1.5 -0.5; 0 1 0 1.5 0  0;     0 0 1  0.5 0    0;...
                1 0 0 0 -1.5  0;   0 1 0 1.5 0 -0.5;   0 0 1  0   0.5  0;...
                1 0 0 0 -1.5  0.5; 0 1 0 1.5 0  0;     0 0 1 -0.5 0    0];
```

C.2.2 Sub-function of *demostructure.m*

```
function [K] = elementstiffness(EA,EIx,EIy,EIz,GI,L,alfa,beta,gama,i)
%=========================================================================
% Elementstiffness matrix and transformation
% Author:  Dimitrij Shulkin, 2012
%=========================================================================
if i <= 2
   EIz = EIx; % Symmetry
elseif (i == 4) || (i == 6) || (i == 8) || (i == 10)
    EIy = EIx; % Symmetry
end;

% Element stiffness matrix
% Freymann R. - Strukturdynamik, Ein Anwendungsorientiertes Lehrbuch, 2011
Kb = [EA/L 0 0 0 0 0 -EA/L 0 0 0 0 0;...                                %u1
      0 12*EIz/L^3 0 0 0 6*EIz/L^2 0 -12*EIz/L^3 0 0 0 6*EIz/L^2;...    %u2
      0 0 12*EIy/L^3 0 -6*EIy/L^2 0 0 0 -12*EIy/L^3 0 -6*EIy/L^2 0;...  %u3
      0 0 0 GI/L 0 0 0 0 0 -GI/L 0 0;...                                %u4
      0 0 -6*EIy/L^2 0 4*EIy/L 0 0 0 6*EIy/L^2 0 2*EIy/L 0;...          %u5
      0 6*EIz/L^2 0 0 0 4*EIz/L 0 -6*EIz/L^2 0 0 0 2*EIz/L;...          %u6
     -EA/L 0 0 0 0 0 EA/L 0 0 0 0 0;...                                 %u7
      0 -12*EIz/L^3 0 0 0 -6*EIz/L^2 0 12*EIz/L^3 0 0 0 -6*EIz/L^2;...  %u8
      0 0 -12*EIy/L^3 0 6*EIy/L^2 0 0 0 12*EIy/L^3 0 6*EIy/L^2 0;...    %u9
      0 0 0 -GI/L 0 0 0 0 0 GI/L 0 0;...                                %u10
      0 0 -6*EIy/L^2 0 2*EIy/L 0 0 0 6*EIy/L^2 0 4*EIy/L 0;...          %u11
      0 6*EIz/L^2 0 0 0 2*EIz/L 0 -6*EIz/L^2 0 0 0 4*EIz/L];            %u12

% Transformation matrix
% Freymann R. - Strukturdynamik, Ein Anwendungsorientiertes Lehrbuch, 2011
tb = [cos(beta)*cos(gama) cos(beta)*sin(gama) -sin(beta);...
      sin(alfa)*sin(beta)*cos(gama)-cos(alfa)*sin(gama)...
      sin(alfa)*sin(beta)*sin(gama)+cos(alfa)*cos(gama) sin(alfa)*cos(beta);...
      cos(alfa)*sin(beta)*cos(gama)+sin(alfa)*sin(gama)...
      cos(alfa)*sin(beta)*sin(gama)-sin(alfa)*cos(gama) cos(alfa)*cos(beta)];

O  = [0 0 0;...
      0 0 0;...
      0 0 0];

Tb = [tb O O O;...
      O tb O O;...
      O O tb O;...
      O O O tb];
% Transformation of element stiffness matrix
K  =   Tb'*Kb*Tb;
```

C.3 Base excitation simulation

```
function[X wr sr s plotnumber] = response_analysis(K,M,G,ub,properties)
%=========================================================================
% INPUT DATA:   reduced system matrices and geometry matrix
% OUTPUT DATA:  eigenvalues, mode shapes and responses
% Author:       Dimitrij Shulkin, 2012
%=========================================================================
%                                EIGENVALUES
%=========================================================================
[x la]      =       eig(K,M);
ff          =       sqrt(la)/(2*pi);
freq        =       zeros(1,30);
for i = 1:30
    freq(i) = ff(i,i);
end;
[f_sort,id] =       sort(freq);
x_sort      =       x(:,id);
f_sort
% Mode Shapes
L           =       properties.L;
dof         =       30;
for s = 1:dof
    plotshapes(x_sort(:,s),L,s,f_sort(s));
end;
b           =       0.001;          % Rayleigh-Damping
Mgen        =       x'*M*x;         % Generalized mass matrix
Ph          =       x*Mgen^(-0.5);  % Mass-normilized eigenvector
%=========================================================================
%                       BASE EXCITATION SIMULATION
%=========================================================================
F           =       -M*G*ub;        % Effective force vector
wr          =       32:0.1:158;     % Limited frequency band
sr          =       length(wr);
% Reduced FRF
Hr          =       zeros(dof,dof*sr);
for j = 1:dof
    for k = 1:dof
        hr   = zeros(dof,sr);
        for n = 1:dof
            hr(n,:)    = hr(n,:)+ wr.^2*(Ph(j,n)*Ph(k,n))./...
                (la(n,n) - wr.^2 + sqrt(-1)*b*la(n,n)*wr);
            Hr(j,((k-1)*sr+1):k*sr)  = Hr(j,((k-1)*sr+1):k*sr)+ hr(n,:);
        end;
    end;
end;
% Reduced acceleration responses
X           =       zeros(dof,sr);
qr          =       zeros(dof,sr);
for j = 1:dof
    for k = 1:dof
    X(j,:) = X(j,:) + F(k)*Hr(j,((k-1)*sr+1):k*sr);
    end;
end;
%=========================================================================
% Presentation of responses: SENSORS C and E
f = wr/(2*pi);
plotnumber = dof+1;
figure(plotnumber);
plot(f,abs(X(7,:)),f,abs(X(8,:)),f,abs(X(9,:)),...
     f,abs(X(13,:)),f,abs(X(14,:)),f,abs(X(15,:)),'linewidth',2);
hold on;xlabel('excitation frequency [Hz]');ylabel('abs. acceleration resonse
[m/s²]');
legend('x7','y8','z9','x13','y14','z15');grid;title('responses');
```

C.3.1 Figures of mode shapes

```
function plotshapes(x,L,j,freq)
%=========================================================================
% Figures of mode shapes
% Author: Dimitrij Shulkin, 2012
%=========================================================================
%                               ORIGINAL FIGURE
%=========================================================================
% X1, Y1, Z1 matrices, plots one or more lines in
% three-dimensional space through the points whose coordinates are the
% elements of X1, Y1, and Z1
X       =       [0 0;0 0;0 L(3);0 0;0 -L(5);0 0;0 L(7);0 0;0 -L(9);0 0];
Y       =       [0 0;0 0;0 0;0 L(4);0 0;0 -L(6);0 0;0 L(8);0 0;0 -L(10)];
Z       =       [0 L(1);L(1) (L(1)+L(2));L(1) L(1);L(1) L(1);L(1) L(1);...
                 L(1) L(1);L(1)+L(2) L(1)+L(2);L(1)+L(2) L(1)+L(2);...
                 L(1)+L(2) L(1)+L(2);L(1)+L(2) L(1)+L(2)];
figure(j)
for i = 1:10
    plot3(X(i,:),Y(i,:),Z(i,:),'LineWidth',1,'Color',[0.7 0.7 0.7],...
                'MarkerEdgeColor',[0 0 0],...
                'MarkerFaceColor',[0 0 0],...
                'MarkerSize',5);
            hold on;
end;
%=========================================================================
%                                 MODE SHAPES
%=========================================================================
x1 = 0.2*x; % Scaling
X1 = [0      x1(1);          x1(1)   x1(4);...
      x1(1)  L(3)+x1(7);     x1(1)   x1(10);...
      x1(1) -L(5)+x1(13);    x1(1)   x1(16);...
      x1(4)  L(7)+x1(19);    x1(4)   x1(22);
      x1(4) -L(9)+x1(25);    x1(4)   x1(28)];

Y1 = [0     -x1(2);          -x1(2)       -x1(5);...
      -x1(2) -x1(8);          -x1(2)   -L(4)-x1(11);...
      -x1(2) -x1(14);         -x1(2)    L(6)-x1(17);...
      -x1(5) -x1(20);         -x1(5)   -L(8)-x1(23);...
      -x1(5) -x1(26);         -x1(5)    L(10)-x1(29)];


Z1 = [0                 L(1)-x1(3);         L(1)-x1(3)      L(1)+L(2)-x1(6);...
      L(1)-x1(3)        L(1)-x1(9);         L(1)-x1(3)      L(1)-x1(12);...
      L(1)-x1(3)        L(1)-x1(15);        L(1)-x1(3)      L(1)-x1(18);...
      L(1)+L(2)-x1(6)   L(1)+L(2)-x1(21);   L(1)+L(2)-x1(6) L(1)+L(2)-x1(24);...
      L(1)+L(2)-x1(6)   L(1)+L(2)-x1(27);   L(1)+L(2)-x1(6) L(1)+L(2)-x1(30)];



% Mode shapes
for i = 1:10
    plot3(X1(i,:),Y1(i,:),Z1(i,:),'--ko','LineWidth',2,...
                'MarkerEdgeColor','k',...
                'MarkerFaceColor',[0 0 0],...
                'MarkerSize',5);
    hold on;
    title([num2str(j) '.mode:  ' num2str(freq) ' Hz']);
    %xlabel('x');
    %ylabel('y');
    %zlabel('z');
    axis equal;
 end;
%[num2str(freq) ' Hz']
```

C.4 *identification.m*

```
function [frr drr]  =   identification(A,B,Au,Bu,G,Omega,plotnumber,effdof)
%=========================================================================
% INPUT DATA:  Measured matrices, geometry matrix, frequency matrix, rankr
% OUTPUT DATA: Eigenfrequenies, mode shapes and damping
% Author:      Dimitrij Shulkin, 2012
%=========================================================================

sr      =   length(Omega);
dof     =   length(G);
wr      =   zeros(1,sr);
for ii  =   1:sr
    wr(ii)  =   Omega(ii,ii);
end;
%=========================================================================
%                       PROCEDURES OF RANK ESTIMATION
%=========================================================================
% Singular value decomposition
[UB SB WB]  =   svd(B,0);
[UA SA WA]  =   svd(A,0);
% Plot of the ratios vs consecutive singular values
ratiob      =   zeros(1,(dof-1));
for i = 1:(dof-1)
    ratiob(i) = (SB(i,i)+1)/(SB((i+1),(i+1))+1);
end;
figure(plotnumber+2)
plot(1:(dof-1),ratiob,'linewidth',3);
hold on;
grid;
title('Ratios of consecutive singular values vs. singular value no.');
xlabel('singular value number');
ylabel('ratio Sj/Sj+1');

% Substitute measuring matrix
effb = 1:dof;
Beff = zeros(dof*sr,dof);
for i = 1:dof
    SBeff=0;UBeff=0;WBeff=0;
    SBeff = SB(1:effb(i),1:effb(i));
    UBeff = UB(:,1:effb(i));
    WBeff = WB(:,1:effb(i));
    Beff((i-1)*sr+1:i*sr,:)= UBeff*SBeff*WBeff';
end;

% RMS
rms = zeros(1,dof);
for r = 0:dof-1
    zb=0;nb=0;
        for i = 1:sr
            for j = dof
            zb = zb + (Beff(r*sr+i,j) - B(i,j))^2;
            nb = nb + B(i,j)^2;
            end;
        end;
    rms(r+1) = sqrt(zb/nb);
end;
rms = rms*100;
figure(plotnumber+3)
plot(1:dof,rms,'linewidth',2);
hold on; title('rms-deviation of substitute measurement rank');
xlabel('estimated rank numbers r');ylabel('rms [%]');grid;
```

```
%=========================================================================
%                         IDENTIFICATION EQUATION
%=========================================================================
SA(effdof+1:dof,effdof+1:dof)   =       0;
SB(effdof+1:dof,effdof+1:dof)   =       0;
Aeff                            =       UA*SA*WA';
Beff                            =       UB*SB*WB';
WBeff                           =       WB(:,1:effdof);
% LEFT SIDE OF EQUATION
LEFT    = [Aeff*WBeff -Omega*Beff*WBeff;...
           Beff*WBeff Omega*Aeff*WBeff];
% RIGHT SIDE OF EQUATION -->> Bu = 0
RIGHT   = [(Omega.^2*Au*G'+Omega.^2*Aeff)*WBeff;...
           (Omega.^2*zeros(sr,6)*G'+Omega.^2*Beff)*WBeff];
%Lest square
MID     =   LEFT\RIGHT;
% Condensed system matrices
KT      =   MID(1:effdof,:);          Krr     =   KT';
CT      =   MID(effdof+1:2*effdof,:); Crr     =   CT';
%=========================================================================
%                       UNDAMPED CONDENSED EIGENPROBLEM
%=========================================================================
[yc Wy] =   eig(Krr);       % right-hand eigenvalue problem
[xc Wx] =   eig(Krr');      % left-hand eigenvalue problem
freqeff =   sqrt(Wy)/(2*pi);% identified eigenfrequencies
% back transformation to physical coordinates
Yc      = WBeff*yc;
Xc      = WBeff*xc;
%=========================================================================
%                           DAMPED EIGENPROBLEM
%=========================================================================
DD      = [zeros(effdof,effdof) -eye(effdof);Krr Crr];
[ksi p] = eig(DD);
%=========================================================================
%                         DAMPING AND EIGENFREQUENCY
%=========================================================================
wrr = zeros(1,2*effdof);
drr = zeros(1,2*effdof);
for i = 1:2*effdof
    wrr(i) = sqrt(real(p(i,i))^2+imag(p(i,i))^2);
    drr(i) = sqrt(real(p(i,i))^2)/wrr(i);
end;
frr = wrr/(2*pi)
%=========================================================================
%                          RECALCULATING RESPONSES
%=========================================================================
mue             = xc'*yc;
beta            = xc'*Crr*yc;
rir             = zeros(dof,sr);
rim             = zeros(dof,sr);
for k = 1:sr
    ai      =   (-wr(k)^2*eye(effdof)+Wy)*mue;
    fire    =   -wr(k)^2*Xc'*G*Au(k,:)';
    fiim    =   -wr(k)^2*Xc'*G*Bu(k,:)';
    Links   =   [ai -wr(k)*beta;wr(k)*beta ai];
    Rechts  =   [fire;fiim];
    Mitte   =   Links\Rechts;
    qreel   =   Mitte(1:effdof);
    qimag   =   Mitte(effdof+1:2*effdof);
    rir(:,k)= Yc*qreel;
    rim(:,k)= Yc*qimag;
end;
f = wr/(2*pi);figure(plotnumber+4);
plot(f,rim(7,:),'--',f,rim(8,:),'--',f,rim(9,:),'--',f,B(:,7),...
            f,B(:,8),f,B(:,9),'linewidth',2);
hold on;xlabel('excitation frequency [Hz]');ylabel('acceleration response [m/s²]');
grid;title('forced responses');legend('x7-ISSPA','y8-ISSPA','z9-ISSPA',...
    'x7-EXACT','y8-EXACT','z9-EXACT');
```

C.4.1 Interface

```
function [A B Au Bu Omega] = interface(X,wr,sr,ub)
%=========================================================================
% Generating of analytical input data of the demo structure for identification
% Author: Dimitrij Shulkin, 2012

dof             =   30;
X1              =   real(X);            % Real part
X2              =   imag(X);            % Imaginary part
A               =   zeros(sr,dof);      % Real matrix
B               =   zeros(sr,dof);      % Imaginary matrix
Au              =   zeros(sr,6);        % Real part excitation matrix
Bu              =   zeros(sr,6);        % Imaginary part excitation matrix
Omega           =   diag(wr);           % Excitation frequency
for j = 1:dof
    A(:,j) = X1(j,:);
    B(:,j) = X2(j,:);
end;
for i = 1:sr
    Au(i,:) = ub';
end;
```